5-1-2014

Simulations of Interfacial Electrokinetics with Applications to Microfluidic Systems

Sebastian Uppapalli
University of Nevada, Las Vegas, uppapall@unlv.nevada.edu

SIMULATIONS OF INTERFACIAL ELECTROKINETICS WITH APPLICATIONS TO MICROFLUIDIC SYSTEMS

by

Sebastian Uppapalli

Master of Science in Mechanical Engineering
University of Nevada, Reno
2003

A dissertation submitted in partial fulfillment
of the requirements for the

Doctor of Philosophy - Mechanical Engineering

Department of Mechanical Engineering
College of Engineering
The Graduate College

University of Nevada, Las Vegas
May 2014

UNLV
UNIVERSITY OF NEVADA LAS VEGAS

THE GRADUATE COLLEGE

We recommend the dissertation prepared under our supervision by

Sebastian Uppapalli

entitled

Simulations of Interfacial Electrokinetics with Applications to Microfluidic Systems

is approved in partial fulfillment of the requirements for the degree of

Doctor of Philosophy in Engineering - Mechanical Engineering

Department of Mechanical Engineering

Hui Zhao, Ph.D., Committee Chair

Yi-Tung Chen, Ph.D., Committee Member

Robert Boehm, Ph.D., Committee Member

Mei Yang, Ph.D., Graduate College Representative

Kathryn Hausbeck Korgan, Ph.D., Interim Dean of the Graduate College

May 2014

ABSTRACT

Simulations of Interfacial Electrokinetics with Applications to Microfluidic Systems

by

Sebastian Uppapalli

Dr. Hui Zhao, Examination Committee Chair
Assistant Professor of Mechanical Engineering
University of Nevada Las Vegas

Electrokinetics plays an important role in facilitating fluid transport and particle manipulation in microfluidic systems. This dissertation studies the mechanics of electrokinetic phenomena for microscale particles and drops. The work aims to increase the understanding of complex electrokinetic phenomena for applications in Lab-on-Chip technology, assembly of colloidal particles and two-phase flow sensing. The standard model consisting of the Poisson-Nernst-Planck equations is used to study the electric double layer polarization of charged dielectric particles and channel wall which plays a major role in control and manipulation of colloidal particles and understanding of electrohydrodynamic flow field.

The cases of polarization of "soft" particle under the influence of alternating current field, influence of residual charges and particle size on electrostatic interaction between charged particles at oil-water interface, and characterization of streaming potential due to drop deformation for a two phase steady flow are modeled and simulated. The theoretical predictions were compared and favorably agree with analytical and experimental observations. The study provides insights to the electrokinetic behavior of micro particles and drops in response to electric fields and pressure driven hydrodynamics respectively. It also helps to quantify the mechanics of colloidal assembly

for monolayered geometry. Implementation of above ideas can improve the designs of devices used for sensing, control and manipulation in microfluidic systems.

ACKNOWLEDGEMENTS

I am indebted to Dr. Hui Zhao, my advisor and chair, for his guidance, support, and understanding. I always left our meetings with a renewed sense of confidence and direction. I would also like to thank my committee members, Dr. Yitung Chen, Dr. Robert Boehm, Dr. Yingtao Jiang, and Dr. Mei Yang for their support and feedback.

I cannot forget Dr. Byard D. Wood, who had a great influence on my educational journey. He is a wonderful role model, and mentor.

Finally, I would like to express my sincere thanks to my parents for their support and prioritizing their children's education over everything else.

Financial support provided by UNLV Innovation Grant and American Chemical Society Petroleum Research Fund is thankfully acknowledged.

DEDICATION

To my wife, Pradnya Hivale,

Thank you for always believing in me and for your support through this journey.

TABLE OF CONTENTS

LIST OF FIGURES

CHAPTER 1

INTRODUCTION

Perspective

"Electrokinetics" refers to the study of electrically driven mechanical motion of charged particles or fluids. Thus, it involves study of electrohydrodynamics ie, the coupling of electromagnetism and hydrodynamics. In this dissertation we only deal with electromagnetic phenomena in electrostatic regime. Sometimes, the term is used more narrowly for fluid or particle motion in electrolytes and ionic liquids.

The microfabrication technology has advanced the microelectronic and computational technologies at amazing speed making Internet and modern telecommunications possible. The enormous potential of this technology has lately been directed towards fields of Mechanical and Bio-Medical engineering, leading to rapid development of Micro-Electrical-Mechanical Systems (MEMS) and Laboratory-on-Chip (LoC) devices.

A LoC device is a microscale chemical or biological laboratory built on thin glass or plastic plate with a network of microchannels, electrodes, sensors and electronic circuits (Li, 2004). Application of electric fields via electrodes along microchannels allows control and manipulation of fluid flow and other operations on the chip. In conventional laboratories, analysis is generally carried out as a series of separate operations using separate tools, techniques and macro-sized instruments requiring large

volume of samples and chemicals. This results in higher operating costs and overheads and longer time for analysis. The LoC device, on the other hand, consists of miniaturized integrated components capable of performing same series of tasks on a single chip. Furthermore, using microfabrication technology, many parallel microchannels can be embedded on a single chip, so that it can perform multiple tasks at any given time. Currently, issues related to higher costs and access in health care are driving the development of such devices.

Similarly to detect and analyze environmental pollutants, water borne pathogens, moisture management in soils, flow rates in industrial piping, water intrusion in oil wells or conversely oil-spill near water reservoirs requires development of micro-sensors that can provide cheap, accurate and on-site analysis of required properties with higher resolution and sensitivity.

In most biomedical and industrial applications, the commonly used media is liquid. Therefore, the key to the functions of LoC and micro-sensors is quantitative control of flow, mass and heat transfers in microchannels. Study of transport processes in microchannels is called microfluidics. Precise manipulation of microfluidic processes is key to proper operation and performance of such sensors and LoC devices. Generally, microscale systems have large surface area to volume ratio and hence the effect of liquid and channel wall interface becomes very significant. Since most solid-liquid interfaces have electrostatic charge and consequently electric fields associated with them, study of interfacial electrokinetic phenomena are very important to microfluidic processes (Li, 2004). In recent years, research towards material assembly using electrokinetic phenomena has led to successful creation of lattice structures at micro scale (Ristenpart,

2003). At present, lack of understanding of complicated electrokinetic transport phenomena at microscales presents a hindrance in development of such advanced technologies.

History

Advances in Electrokinetics can be divided into two categories. One concerning Theoretical Modeling and another concerned with fabrication.

Electrokinetic phenomena belong to the oldest areas of surface and colloid science. Only surface tension and related concepts have a longer history, dating from the time of Francis Hauksbee, Newton's assistant at the Royal Society. The discovery of the electrokinetic phenomena electrophoresis, electro-osmosis, and streaming potential, gave rise to the concept of the electrical double layer (Wall, 2009). In 1808, Reuss first observed the electrokinetic phenomena when he applied a Direct Current to clay water mixture. Later, in 1846 Napier made a distinction between Electro-osmosis and Electrophoresis. It was Helmholtz, in 1879, who developed the first analytical model to describe electrokinetic phenomena. Finally, Pellat in 1904 and Smoluchowski in 1921 developed an extension to Helmholtz model to derive electrokinetic velocity.

Richard Feynman's lecture in 1959 regarding miniaturization and successive invention of microfabrication technology to fabricate electronic chips, scientific and commercial advances in the field of microsystem technology has been tremendous. In the late 1970s, this technology was extended to machining mechanical microdevices leading to development of MEMS.

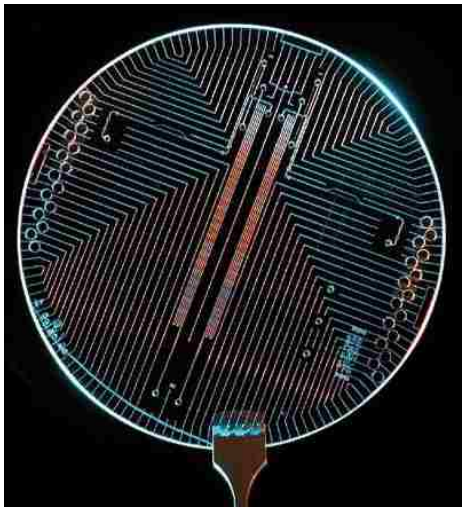

Figure 1 Image of a sample fluidic network (Courtesy: Mathies lab, UC Berkley).

The development of microflow sensors, micropumps, and microvalves in the late 1980s constituted the early stage of microfluidics. Since then, the field has rapidly developed when it was realized that the main application fields of microfluidics are life sciences and chemistry (Manz et. al., 1989).

In the mid-1990s, microfluidics was applied as a research tool in the field of genomics. Later DARPA provided research support, to realize portable bio-chemical warfare detection systems, pushing microfluidics into mainstream RD&D field. This is indicated by Figure 2 that shows an exponential increase of papers on microfluidics in subsequent years.

Surface Phenomena

Generally, we may classify the transport processes into three categories according to the characteristic dimension, L_c of the systems:

1. Macroscale systems - $L_c > 200\mu m$
2. Microscale systems - $100nm < L_c < 200\mu m$
3. Nanoscale systems - $L_c < 100nm$

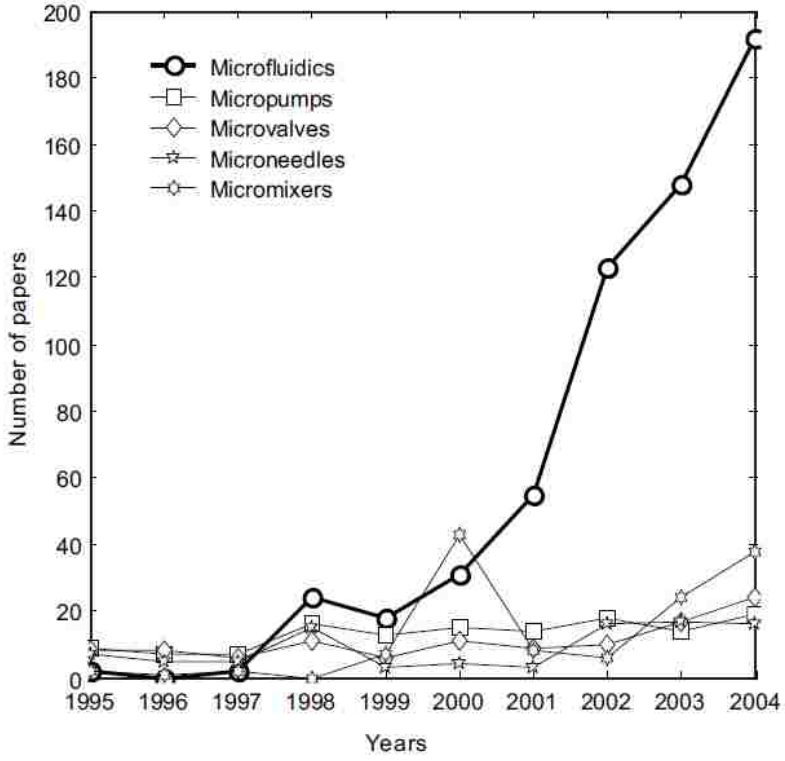

Figure 2 Publication of microfluidic related papers (Nguyen & Wereley, 2006).

Because of large surface-to-volume ratio in microchannels, the surface properties become enormously important. For example, a microchannel of $100\mu m$ diameter, has a surface-to-volume ratio (S/V) of $2 \cdot 10^4 m^{-1}$. Thus, for fluid flows in microchannels (Conlisk, 2013):

1. Surface properties like, charge, roughness, hydrophobicity etc. have significant effect on fluid flow.
2. Significant fluid slip may occur at wall, if the surface is hydrophobic.
3. The continuum approximation may break down, especially for compressible flows.
4. Molecular diffusion, which is very slow at macroscale, becomes very fast at micro and nanoscales.
5. Pressure driven flow is only viable for very low flow rates $\sim 1nL/\min$.

It becomes increasingly difficult to pump liquids by pressure in microchannels because pressure gradient scales as $\Delta p \sim 1/h^3$. Thus, fluid, biomaterials and other particles are often transported electrokinetically. Figure 3 below shows various sizes of microfluidic devices.

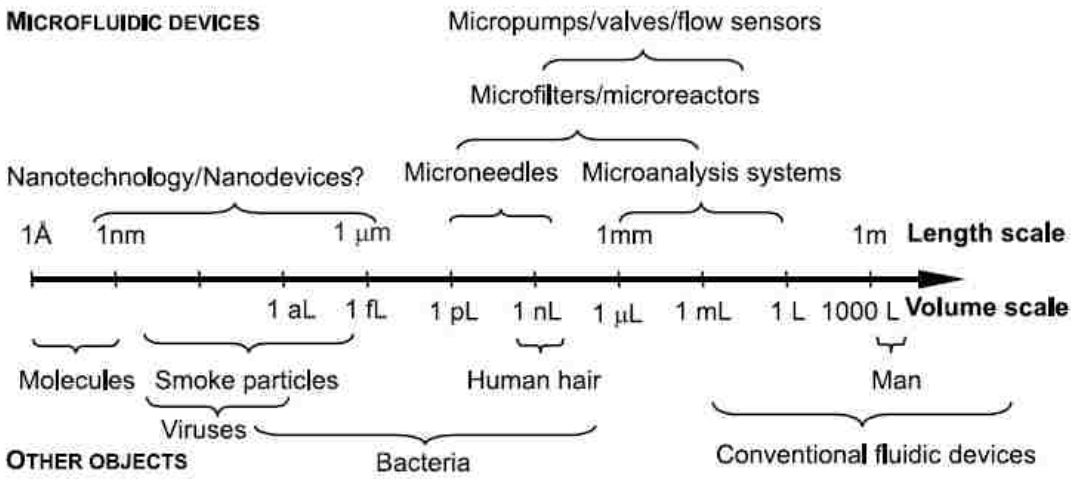

Figure 3 Size characteristics of microfluidic devices (Nguyen & Wereley, 2006).

Applications

The major applications, of microfluidics and associated electrokinetic phenomena are in biotechnology, nanotechnology, pharmaceutical, food processing and environmental monitoring industry. Medical diagnostics (in lab or point-of-care), genetic sequencing, chemistry production, and environmental monitoring are some of the examples where microfluidics has been successfully applied at commercial level. Concurrent with the exploration of new effects, microfluidics today is looking for further application fields beyond conventional fields, such as flow control, chemical analysis, biomedical diagnostics, and drug discovery. New applications utilizing microfluidics for distributed energy supply (fuel cells and capacitors), distributed thermal management, and chemical production are promising. Chemical production using distributed microreactors makes new products possible. The large-scale production can be realized easily by running multiple identical microreactors in parallel. Scalability is inherent in microfluidics, and can be approached from the point of view of "numbering up" rather than scaling up (Nguyen & Wereley, 2006).

In biotechnology, the most highly developed applications are probably their use to screen conditions (such as pH, ionic strength and composition, co-solvents, and concentration) for protein crystallization. Other applications for which there are laboratory demonstrations include separations coupled to mass spectroscopy, high-throughput screening in drug development, bioanalyses, examination and manipulation of samples consisting of a single cell or a single molecule.

The manipulation of multiphase flows is another strength of microfluidic systems. They enable the generation and manipulation of monodisperse bubbles or droplets of a dispersed gas or liquid phase in a continuous liquid stream providing new pathways to generate particles and emulsions. Droplets can also serve as compartments in which to study fast organic reactions (Whitesides, 2006). Similarly, non-linear electrokinetics has been successfully used in laboratory environment to create lattices and various patterns of particle assembly. Such assemblies can be controlled and manipulated to develop new materials with specific electrical, mechanical and optical properties (Zhao, 2012). Electrokinetic phenomena, historically, has found wide applications in geotechnical engineering (Shang, 2011) and recently, in capacitive desalination and bubble removal in additive manufacturing.

Current Status

Initially, microfluidics developed as a part of MEMS technology, which in turn used the established technologies and infrastructure of microelectronics. Fluid mechanics researchers are interested in the new fluids phenomena possible at the microscale. In contrast to the continuum-based hypotheses of conventional macroscale flows, flow physics in microfluidic devices is governed by a transitional regime between the continuum and molecular-dominated regimes. Besides new analytical and computational models, microfluidics has enabled a new class of fluid measurements for microscale flows. Microfluidic tools allow Life Scientists and chemists to explore new effects not possible in traditional devices. These new effects, new chemical reactions, and new

microinstruments lead to new applications in chemistry and bioengineering. These reasons explain the enormous interest of research disciplines in microfluidics. Nowadays, almost all conferences of professional societies, such as the Institute of Electrical and Electronic Engineers (IEEE), American Society of Mechanical Engineers (ASME), International Society for Optical Engineering (SPIE), and American Institute of Chemical Engineers (AIChe), have technical sessions for microfluidics.

With relatively recent accomplishments in the Human Genome Project and huge potential in the fields of biotechnology and nanotechnology, microfluidic devices have the potential to be a commercial success. The apparent interest and participation by industry in microfluidics research and development shows commercial potential of microfluidic devices for practical applications.

Scope of the Dissertation

This dissertation aims to improve understanding of complex electrokinetic phenomena by modeling and simulating the influence of interfacial electrokinetics; (1) in controlling and manipulating microscale particles, as applicable to biomedical separation and sorting and material assembly and (2) in development of a two-phase flow sensor by characterizing microscale droplet deformation in a two component flow.

In all three cases, the modeling meets three specific criteria:

1. Apply standard theoretical model developed from first principles.

2. Validate the results from simulations with established results, either experimental or analytical.
3. Understand influence of various electrokinetic properties governing the physical phenomena.

In this regard, the dissertation is organized as follows. Chapter 2 presents the fundamental principles governing electrokinetic phenomena and discusses various types of electrokinetic phenomena. In Chapter 3, Polarization of a soft particle under the action of AC electric fields with applications to dielectrophoresis is studied. Chapter 4 discusses the influence of surface charges and particle size on electrostatic interactions between colloidal particles at oil-water interface and chapter 5 presents characterization of droplet deformation in a two-phase flow. Chapter 6 concludes.

CHAPTER 2

FUNDAMENTALS OF ELECTROKINETICS

Introduction

Electrokinetic phenomena are a family of several different physicochemical effects that occur in electrolytes, ionic and dielectric liquids. There is a common source for these effects, the so called Interfacial Double Layer or Electric Double Layer (EDL) that appears on the surface of an object when it is exposed to a fluid. Influence of external force on EDL generates tangential motion with respect to charged surface (Bruus, 2007). As discussed in the previous chapter, that as the typical length scale of the system approaches micro scale level and smaller, pressure driven transport, becomes increasingly difficult and electrokinetic phenomena are often used for transporting charged and uncharged species and biomolecules at micro and nano scales (Conlisk, 2013). Here we briefly review the basic governing equations, as well as several types of electrokinetic phenomena.

Governing Equations of Incompressible Fluids

For an incompressible fluid like water, the governing equation is the Navier-Stokes equation which takes the non-dimensional form as (Fox et. al., 2011)

$$\frac{\partial \vec{u}}{\partial t} + \vec{u} \cdot \nabla \vec{u} = -\nabla p + \frac{1}{\mathrm{Re}} \nabla^2 \vec{u} + f \tag{2.1}$$

where, $\mathrm{Re} = \frac{uL}{\nu}$ is the Reynolds number, u, p, f, ν and L is the velocity, pressure, the external force, kinematic viscosity and characteristic length respectively. In micro and nano systems, where $\mathrm{Re} << 1$ because of smaller length scales, the non-linear terms can be neglected and the governing equation reduces to Stokes equation which takes the form as (Morgan & Green, 2003)

$$Sc\frac{\partial \vec{u}}{\partial t} = -\nabla p + \nabla^2 \vec{u} + f \tag{2.2}$$

where, $Sc = \frac{\nu}{D}$ is the Schmidt number and D is the mass diffusivity. Stokes equation is relatively easier to solve due to linearity of u as compared to Navier-Stokes equation.

Basic Concepts in Electrostatics

Gauss's law states that "the total electric flux through any closed hypothetical surface of any shape drawn in an electric field is proportional to the total electric charge enclosed within the surface". Mathematically, Gauss's law takes the form of an integral equation (Popovic, 1971; Stratton, 2007):

$$\oint_s \vec{E} \cdot ds = \frac{1}{\varepsilon_0}\int \rho_{el} dV = \int \nabla \cdot \vec{E} dV \tag{2.3}$$

where, $\vec{E}$ is the electric field, ρ_{el} is volume charge density and ε_0 is the permittivity of vacuum. Applying Divergence theorem, Gauss's law can be writtn in differential form as

$$\nabla \cdot \vec{E} = \frac{\rho_{el}}{\varepsilon_0} \tag{2.4}$$

The validity of the electrostatic approximation rests on the assumption that the electric field is irrotational:

$$\nabla \times \vec{E} = 0 \tag{2.5}$$

Because the electric field is irrotational, it is possible to express the electric field as the gradient of a scalar function, φ, called the electrostatic potential. An electric field, $\vec{E}$ points from regions of high electric potential to regions of low electric potential, expressed mathematically as

$$\vec{E} = -\nabla\varphi \tag{2.6}$$

From equations 2.4 and 2.6 we can derive Poisson's equation given as

$$\nabla^2\varphi = -\frac{\rho_{el}}{\varepsilon_0} \tag{2.7}$$

In the absence of unpaired electric charge, Poisson's equation reduces to Laplace's equation.

$$\nabla^2\varphi = 0 \tag{2.8}$$

Conservation of Species

Computing fluxes of ions in non-equilibrium situations requires development of models that relate flows to forces in ionic solutions. Motion of chemical species in a fluid medium is a function of ion fluxes due to diffusion, ion migration under the influence of electrostatic forces and velocity gradients of ions (Johnston & Wu, 1995).

Fick's law of diffusion describes ion flux due to concentration gradient

$$j = -D\nabla c \tag{2.9}$$

where, D is the diffusion coefficient and c is the species concentration.

To determine flux due to electrostatic forces, consider the situation of an ionic solution of uniform concentration with a potential gradient given by $\nabla\varphi$. The field will produce a force on a charge q equal to $-q\nabla\varphi$. The charge q carried by a mole of ions is given by $z_i F$, where F , is the Faraday's constant and z_i is the valence of ions. So the force on a mole of ions due to the electric field is $-z_i F\nabla\varphi$. In an aqueous solution, the interactions of solute and solvent molecules result in transport processes being limited largely by the equivalent of frictional forces; since at low $\mathrm{Re} << 1$, viscous forces dominate inertial forces. Thus when an ion is acted on by an electric field, it tends to move with a drift velocity that is proportional to the force provided by the field. This proportionality is the ion mobility m_i. Thus, ionic flux could be written as

$$j = -m_i c z_i F\nabla\varphi \tag{2.10}$$

Similarly, ionic flux due to velocity is simply

$$j = c\vec{u}_i \tag{2.11}$$

where, $\vec{u}_i$ is the ion velocity due to random thermal motion and fluid velocity.

These fluxes when applied to control volume, lead to generalized form of the Nernst-Planck equation which, in the presence of chemical reaction, is a conservation of mass equation.

$$\frac{\partial c}{\partial t} = -\nabla.[-D\nabla c + c\vec{u}_i - D\frac{ze}{k_B T}c\nabla\varphi] + R_r \tag{2.12}$$

Here, $m_i = \frac{D}{RT}$ and $F = \frac{eR}{k_B}$. R is the universal gas constant, e is the charge of an electron, k_B is the Boltzmann constant and R_r is the rate of chemical reaction.

Dipole Moment and Polarization

When a dielectric material is subjected to an external uniform electric field, it becomes polarized. Polarization occurs due to locally induced dipole moments as the bound charges in the material slightly separate, as shown in Figure 4. Electric dipole moment is a measure of separation of positive and negative charges in a system or in other words measure of system's polarity. For a simple case of two point charges $+q$ and $-q$ the dipole moment is given as $p = qd$ where, d is the displacement vector measured from negative charge to positive charge. The aggregate effect of these local dipoles is to produce a spatially dependent moment per unit volume or polarization P (Herczyński, 2013) given as

$$d\vec{p} = \vec{P}dv \tag{2.12}$$

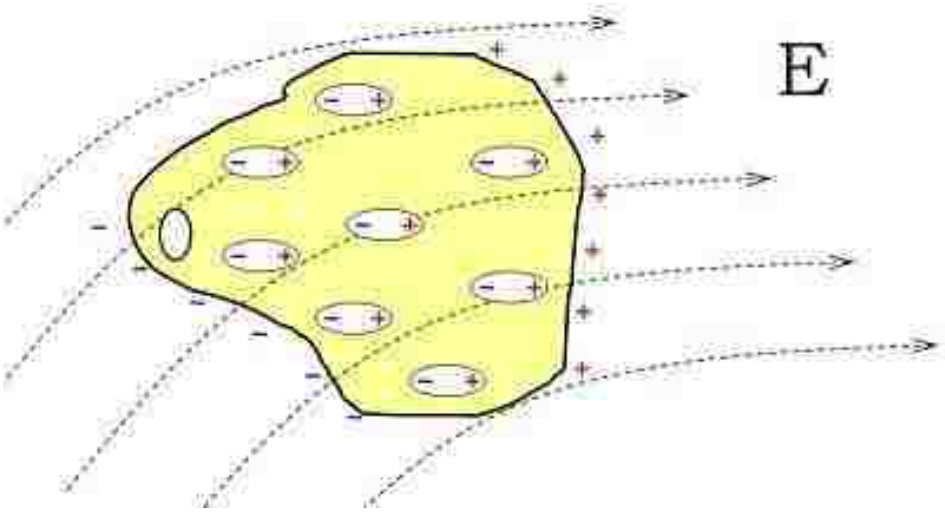

Figure 4 Polarization of a dielectric material.

For a linear, homogeneous, isotropic dielectric material, polarization is linearly dependent on the electric field as (Feynman, 1964)

$$\vec{P} = \varepsilon_0 \chi \vec{E} \tag{2.13}$$

where $\chi = \varepsilon_r - 1$. χ is the susceptibility of the material and ε_r is the relative permittivity of the material. Separating total volume charge density into free and bound charges we can write

$$\rho_{el} = \rho_{el\,f} - \nabla \cdot \vec{P} \tag{2.14}$$

From equation 2.4 and 2.14 we get

$$-\nabla \cdot (\varepsilon_0 \vec{E} + \vec{P}) = \rho_{el\,f} \tag{2.15}$$

Substituting equation 2.13 in equation 2.15 we get the Poisson's equation for a linear, isotropic, dielectric material.

$$\nabla^2 \varphi = -\frac{\rho_{el\,f}}{\varepsilon_0 \varepsilon_r} \tag{2.16}$$

Basics of electric double Layer

Consider an electrolyte in contact with a solid surface. This could be in the form of a channel wall or a solid particle suspended in the liquid. Depending on chemical composition, of solid and liquid, chemical processes on the surface will result in charge transfer [Kirby, 2009]. This is often because of ionic adsorption. Aqueous solutions universally contain positive and negative ions (cations and anions, respectively), which interact with partial charges on the surface, adsorbing to and thus ionizing the surface and creating a net surface charge. This net charge results in a electrostatic field, which causes the surface to be surrounded by a cloud of counter-ions from the bulk. The counterions are influenced by potential gradient and thermal motion creating an ion/counterion layer which extends from the surface into the solution. The larger the partial charges in the material, the more ions are adsorbed to the surface and larger the cloud of counter-ions. A solution with a higher concentration of electrolytes also decreases the size of the counter-ion cloud. This ion/counterion layer is known as the electric double layer (EDL), presence of which screens the surface charge [Kirby, 2009]. Figure 5 below shows a sketch of the EDL.

EDL is composed of two distinct layers: a fixed layer called Stern layer, composed of counterions strongly adsorbed on to the surface and another, slightly mobile layer called Diffuse layer composed of mixture of coions and counterions. The ions in diffuse layer can move under tangential stress since they are not strongly adsorbed to the Stern layer. The double layer is formed in order to neutralize the charged surface and, in turn, causes an electrokinetic potential between the surface and any point in the bulk fluid. This voltage difference is on the order of millivolts and is referred to as the Surface potential. The magnitude of the surface potential is related to the surface charge and the thickness of the double layer [Bruus, 2007].

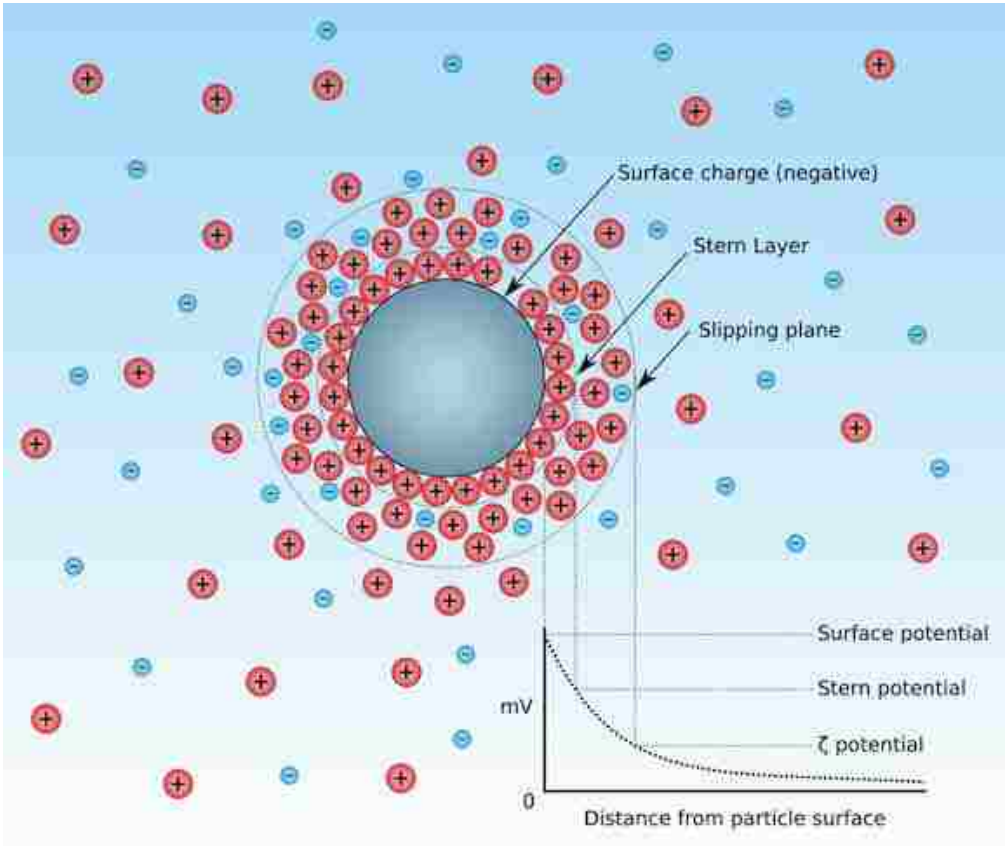

Figure 5 Electric Double Layer around a spherical particle.

As we leave the surface, the potential drops off roughly linearly in the Stern layer and then exponentially through the diffuse layer, approaching zero at the imaginary boundary of the double layer. The potential curve is useful because it indicates the strength of the electrical force between particles and the distance at which this force comes into play. The plane separating the diffuse layer and the Stern layer is called Slipping plane and electric potential at this plane is called Zeta or Electrokinetic Potential, ζ . This potential relates to the mobility of the particle. Although zeta potential is an intermediate value, it is sometimes considered to be more significant than surface potential as far as electrostatic repulsion is concerned.

The characteristic thickness of EDL is called Debye length, λ_D. The non-dimensional Debye length, can be derived using potential scale $\mp\hat{\varphi} = \mp\frac{F}{RT}\varphi$, concentration scale $\hat{c}_\pm = \frac{c_\pm}{c_0}$ and characteristic length scale, L_c. For weak solutions, co and counterions can be modeled as an ideal gas. This allows ionic concentrations near a charged surface to be modeled according to the Boltzmann distribution, which comes from the thermodynamic expression for chemical potential [Bruus, 2007].

$$c_\pm = c_0 e^{\frac{\mp ze}{k_B T}\varphi} \text{ or } \hat{c}_\pm = e^{\mp\hat{\varphi}} \tag{2.18}$$

where, $\mp\hat{\varphi} = \mp\frac{F}{RT}\varphi$, $k_B = \frac{eR}{F}$, $z_\pm = \pm 1$ and $\hat{c}_\pm = \frac{c_\pm}{c_0}$. Charge Density thus can be expressed as

$$\rho_{el} = z_i F c_{i_\pm} = z_i F c_{i\,0}\hat{c}_\pm \tag{2.19}$$

Evaluating net charge density form equations 2.16 and 2.19, we get

$$\nabla^2 \hat{\varphi} = -\frac{\hat{c}_- - \hat{c}_+}{2\hat{\lambda}_D{}^2} \tag{2.20}$$

where, $\hat{\lambda}_D = \frac{\lambda_D}{L_c} = \frac{1}{L_c}\sqrt{\frac{\varepsilon_0 \varepsilon_r RT}{F^2 c_0}}$ is the non-dimensional Debye length. The EDL thickness usually varies from 1 nm to 100 nm.

Poisson-Nernst-Planck Model

The earliest model of EDL is usually attributed to Hermann Von Helmholtz. He treated the EDL, mathematically as a simple capacitor, based on a physical model in which a single layer of ions is adsorbed at the surface (Helmholtz, 1853). Later Louis Georges Gouy and David Chapman introduced a diffuse model of the EDL, in which the electric potential decreases exponentially away from the surface to the bulk. This model fails for highly charged EDLs. In order to resolve this problem Stern suggested the combination of the Helmholtz and Gouy-Chapman models, giving an internal Stern layer and an outer diffuse layer (i.e. Gouy-Chapman layer) (Lyklema, 1995).

The combined Gouy-Chapman-Stern or Modified Gouy-Chapman or nonlinear Poisson-Nernst-Planck (PNP) model is most commonly used. The PNP model makes certain assumptions [Conlisk, 2013]:

- Ions are assumed as point charges.
- Coulombic interactions dominate in diffuse layer of the EDL.

- Dielectric permittivity is assumed constant throughout the EDL.
- Viscosity is constant beyond the EDL and into the bulk fluid.

The PNP model, as the name suggests, consists of coupled Poisson's Equation (equation 2.7) and Nernst Planck equations (equation 2.12). The coupling variables are the electrostatic potential φ and ionic concentration c.

Electro-osmosis

Electro-osmosis (EO) is the bulk motion of fluid caused by an electric field. When electric fields are applied across a porous plug, a capillary or a micro channel, bulk fluid motion is observed. This motion is linearly proportional to the strength of applied electric field and chemical nature of the surfaces and fluid [Kirby, 2009]. It is result of the force exerted by the applied electric field on counterions in the fluid inside charged pores, capillaries etc. The moving ions drag the liquid along with them causing bulk to flow as shown in Figure 6.

The electro-osmotic flow is driven by placing the electrodes in upstream and downstream section of the flow. The charge separation at the walls leads to the formation of EDL. Application of electric field induces a force on EDL, given by $F = \rho_{el} E$, that begins to move and then by viscous drag pulls the neutral bulk liquid along. The continuation of this process is highly dependent on formation of EDL at the electrodes, which would screen the applied electric field. This can be avoided, if electrolysis occurs

at the electrodes which prevents charge accumulation and allows electric current to flow in the system. The current flow would then move the liquid by viscous drag.

The Stokes equation, in combination with Poisson's equation (2.16), can be used to analyze the EO flow, with the Coulomb force included as the body force term of the Stokes equation.

$$\rho(\frac{\partial \vec{u}}{\partial t}) = -\nabla p + \mu \nabla^2 \vec{u} + \rho_{el} \nabla \varphi \tag{2.21}$$

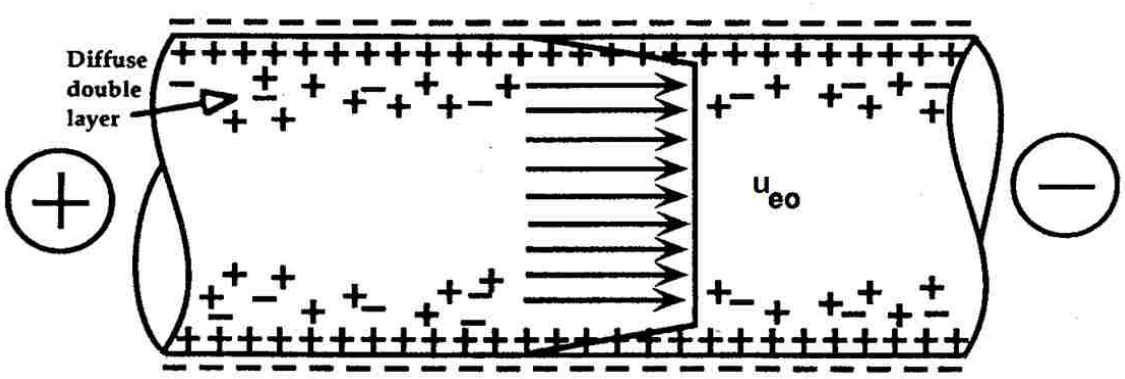

Figure 6 Electro-osmotic flow in a channel.

To determine electro-osmotic velocity, consider a simple case of a channel, with charged surface and tangentially applied electric field. Ideal EO flow is defined by following four conditions:

1. Applied electric field is homogeneous throughout the system.
2. Flow is steady state.

3. ζ potential is constant along the surface.

4. EDL thickness is much smaller than the radius or half-height of the channel.

For a zero external pressure gradient, at the leading order, the dominant balance is between viscous and electrical forces in the EDL (Ghosal, 2004)

$$\mu \nabla^2 u_{eo} + \rho_{el} \nabla \varphi = 0 \tag{2.22}$$

On eliminating ρ_{el} between equations (2.16) and (2.22), integrating the resulting differential equation and using the boundary conditions at the inner and outer edges of the EDL, $u = 0; \varphi = \zeta$ respectively, the following jump condition across the EDL is derived for a limiting case of thin EDL.

$$\vec{u} = -\frac{\varepsilon_0 \varepsilon_r \zeta}{\mu} \nabla \varphi \tag{2.23}$$

In microfluidic applications where the thin EDL assumption applies, it is evident that the velocity of electro-osmosis does not depend on the channel dimensions. This unique feature is strikingly different from the pressure-driven flow in which the velocity depends strongly on channel dimensions. Consequently, the electro-osmotic pumping has long been an efficient and popular technique for fluid transportation in microfluidic devices. This flow, however, is sensitive to chemical features at the interface, and the act of applying electric fields can also move particles relative to the fluid or cause Joule heating (*i.e.*, resistive heating) throughout the fluid.

Electrophoresis

The term "electrophoresis" describes the phenomenon in which dispersed (colloidal) particles move relative to a fluid under the influence of a spatially uniform electric field, either DC or very low frequency AC fields. Consider a particularly simple case of electrophoresis. A charged spherical particle of radius a and charge q, where q is the surface charge, is freely suspended in a stationary liquid of low conductivity, like say deionized water, as shown in Figure 7. Lack of ions in the liquid would result in lack of charge accumulation on the surface of the particle. Thus, an applied electric field will create a Coulombic force, $F_{el} = q\nabla\varphi$ acting on the particle. In a short time scale, this charged particle will reach a steady state motion or electrophoretic velocity due to viscous drag. In this case Stokes drag force $F_{drag} = \frac{-6\pi\mu a}{\rho} u_{ep}$ balances the Coulombic force, giving electrophoretic velocity as

$$u_{ep} = \frac{q\rho}{6\pi\mu a}\nabla\varphi \tag{2.24}$$

This dependence of drift velocity on particle charge and size make electrophoresis particularly suitable for sorting and separation applications (Hunter, 1989).

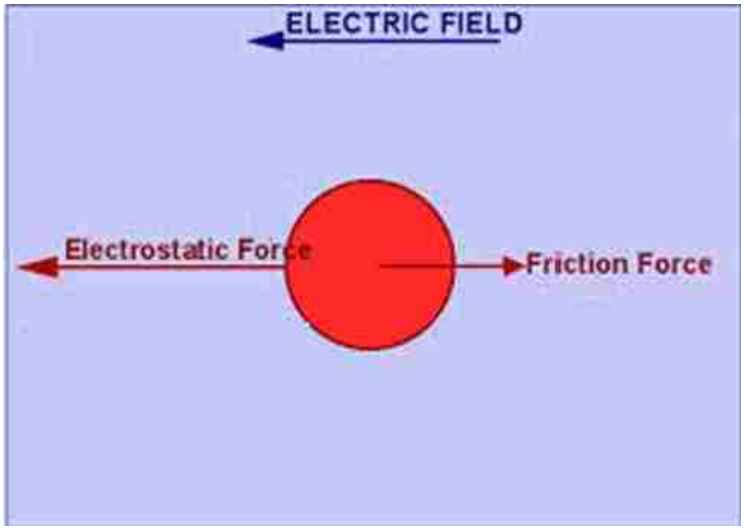

Figure 7 Electrophoretic force on a particle in absence of EDL.

A charged particle freely suspended in an electrolyte solution, will develop an EDL. The electro-osmotic velocity, created by the applied electric field, will also give rise to electrophoretic velocity opposite to the electro-osmotic velocity. Under the limit of the thin double layer, the electrophoretic velocity is given by Smoluchowski equation.

$$\vec{u}_{ep} = \frac{\varepsilon_0 \varepsilon_r \zeta}{\mu} \nabla \varphi \tag{2.25}$$

where, $\frac{\varepsilon_0 \varepsilon_r \zeta}{\mu}$ is the electrophoretic mobility.

The Smoluchowski equation is only valid for thin EDL and for very low surface potential. Henry generalized the Smoluchowski equation for any thickness of EDL by inserting a smooth continuous function $f(\frac{a}{\lambda_D})$. The electrophoretic velocity, equation 2.26, thus obtained is valid for all EDL thicknesses but limitation of small surface potential still applies.

$$u_{ep} = +\frac{\varepsilon_0 \varepsilon_r \zeta}{\mu} \nabla\varphi \cdot f(\frac{a}{\lambda_D}) \tag{2.26}$$

A more complete description of electrophoresis must account for EDL distortion. Figure 8 shows the forces active on a charged spherical particle in an electrolyte solution. As discussed above, Electrostatic or Coulombic force arises from charged particles response to the applied electric field and Friction force is the viscous drag in the solution. The electrophoretic retardation force, accounted by the Henry's equation above, adds to the viscous drag. The ions in EDL respond to applied field in a manner similar to the particle, meaning co-ions tend to migrate in the direction of charged particle whereas counterions tend to migrate in opposite direction. Since there is higher concentration of counterions in the EDL, their migration adds to the viscous drag. The remaining applicable force is called the electrophoretic relaxation force. In the absence of the applied electric field, the center of positive and negative charges in the EDL is coincident. When the electric field is applied, the charged particle migrates relative to the mobile part of the EDL creating a net separation of charges. Conduction and diffusion require finite time to restore symmetry ie, relaxation time. As long the field is applied, the force separating the charges is present and a steady state separation is reached. The resulting dipole exerts an additional drag further inhibiting the particle's motion in response to the applied field. Relaxation is negligible for very thick or very thin EDLs but can be a significant effect at intermediate ranges. This implies non-linear dependence of electrophoretic mobility at higher surface potentials (Aicart et. al., 2006).

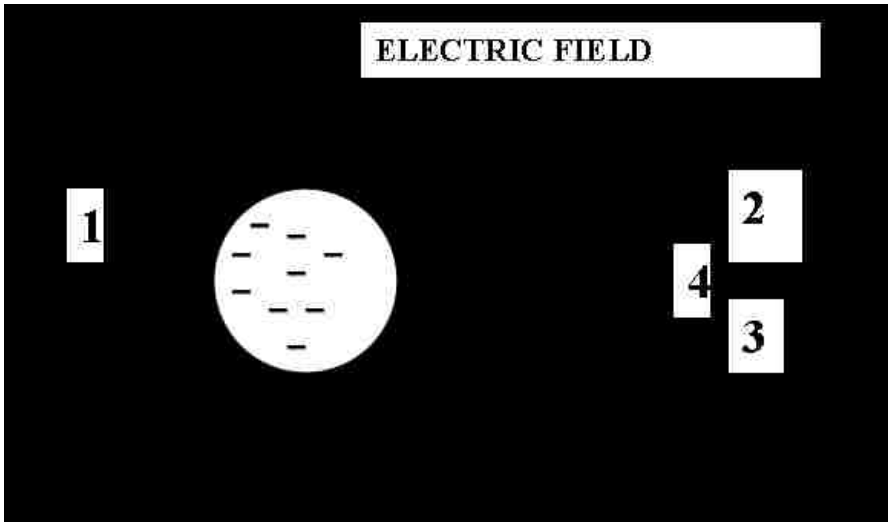

Figure 8 Electrophoretic forces on a charged particle in the presence of EDL. 1: Electrostatic force; 2: Viscous Drag; 3: Electrophoretic retardation; 4: Electrophoretic relaxation.

The vast applications of electrophoresis are most evident in the health or medical industry. Examples include Antibiotic, vaccine, protein and DNA analysis.

Dielectrophoresis

The term dielectrophoresis (DEP) was first introduced by Pohl to describe translational motion of particles due to application of non-uniform electric fields. The dielectrophoretic motion is determined by the magnitude and polarity of the charges induced in a particle by the applied field. Usually DEP is performed under alternating current (AC) fields over wide range of frequencies. The DEP force is dependent on several parameters: the dielectric properties and size of particle, frequency of the applied field and electrical properties of the medium (Pohl, 1978).

To determine dielectrophoretic force or DEP force or F_{DEP}, the first steps involve evaluating the polarization of particle in terms of an equivalent induced dipole moment or effective dipole moment and the electrical potential arising from it (Jones, 1995). The effective dipole moment method can be used to calculate electromechanical forces and torques exerted by electric fields on particles. Indeed, it has been popularly used because of its simplicity and ability to provide meaningful insights in many important situations (Krupke et al., 2003; Morgan & Green, 2003; Dimaki & Bøggild, 2004; Li et al., 2005).

The effective dipole moment, p_{eff} of the particle is defined as the moment of an equivalent, free-charge, point dipole that, when immersed in the same dielectric liquid and positioned at the same location as the center of the original particle, produces the same dipolar electrostatic potential (Jones, 1995). As a result of the spherical geometry and the lossless nature of the dielectric, this induced dipole moment will be aligned with the original external field E. Thus, for all space outside the sphere, the field created by this dipole is superposed onto the field E.

Using the potential form of two equal but opposite charges separated by an infinitesimal distance and applying Taylor expansion, the potential can be expressed as a series, approximated as:

$$\varphi(r,\theta) = \frac{1}{4\pi\varepsilon_m} \cdot p_{eff} \cdot \frac{\cos\theta}{r^2} \tag{2.27}$$

where θ and r are respectively the polar angle and radial position in spherical coordinates (Pethig, 2010). If the dipole is small as compared to the length scale of the

non-uniformity of the imposed field then the force acting on the dipole can be approximated as:

$$F_{DEP} = p_{eff} \cdot \nabla E \tag{2.28}$$

Now consider an isotropic, inhomogeneous, dielectric spherical particle of radius a of absolute dielectric permittivity ε_2 and conductivity σ_2 suspended in an electrolyte of absolute dielectric permittivity ε_1 and conductivity σ_1 subjected to an external non-uniform or AC field $Ee^{i\omega t}$, as shown in Figure 9.

Far from the particle; $r > a$

$$\varphi_1 = -E_0 r\cos\theta e^{i\omega t} + \frac{A\cos\theta}{r^2} E_0 e^{i\omega t} \tag{2.29}$$

Where, the second term on the right hand side of equation 2.29, is due to dipole moment of particle.

On the particle surface; $r = a$

Electrostatic potential at the surface is continuous;

$$\varepsilon_2 \frac{\partial \varphi_2}{\partial n} = \varepsilon_1 \frac{\partial \varphi_1}{\partial n} \tag{2.30}$$

Conservation of charge in electric current flow;

$$J_{r_2} - J_{r_1} + \frac{\partial \sigma_f}{\partial t} = 0 \tag{2.31}$$

where, $J_{r_i} = \sigma_i E_{r_i}$ and free surface charge $\sigma_f = \varepsilon_1 E_{r_1} - \varepsilon_2 E_{r_2}$

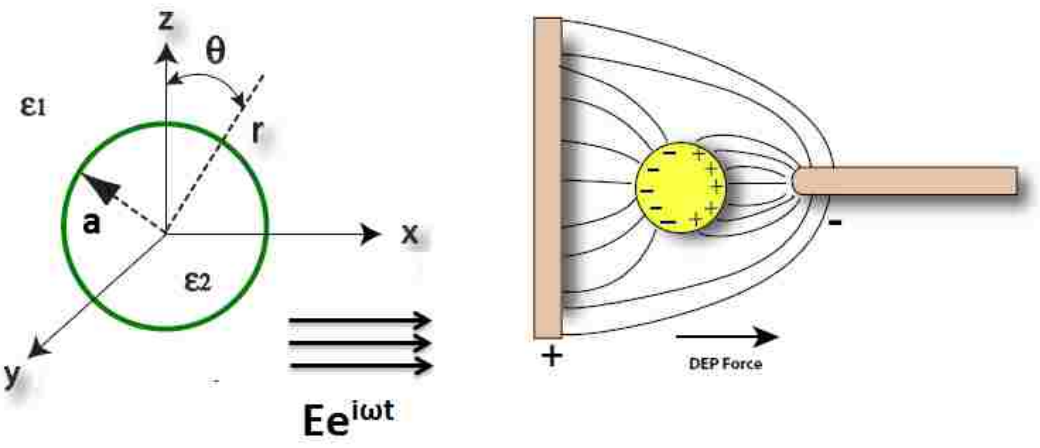

Figure 9 Dielectrophoretic force acting on a spherical particle.

From equations 2.29, 2.30 and 2.31 we can compute coefficient A as:

$$A = \frac{\varepsilon_2^* - \varepsilon_1^*}{\varepsilon_2^* + 2\varepsilon_1^*} a^3 \tag{2.32}$$

where, $\bar{\varepsilon}_i^* = \varepsilon_i^* - i\frac{2\pi\sigma_i^*}{\omega^*}$ is the complex permittivity. From equation 2.27 we can write (Jones, 1995)

$$p_{eff} = 4\pi\varepsilon_1 A \tag{2.33}$$

Thus dielectrophoretic force can be given as:

$$F_{DEP} = 4\pi\varepsilon_1 K a^3 \nabla E^2 \tag{2.34}$$

where, $K = \frac{\varepsilon_2^* - \varepsilon_1^*}{\varepsilon_2^* + 2\varepsilon_1^*}$ is the Clausius-Mossotti factor.

When the applied electric field polarizes the particle, the poles experience DEP force along the field lines, which can be either attractive or repulsive according to the orientation on the dipole. Since the field is non-uniform, the pole experiencing the greatest electric field will dominate over the other, and the particle will move. The orientation of the dipole is dependent on the relative polarizability of the particle and medium. Since the direction of the force is dependent on field gradient rather than field direction, highly polarizable particle will move in the direction of increasing electric field causing positive DEP or pDEP and particles with low polarization will move in direction of decreasing field causing negative DEP or nDEP, shown in Figure 10 (Chang & Yeo, 2009).

Dielectrophoresis can be used to manipulate, transport, separate and sort different types of particles. Since biological cells have dielectric properties, dielectrophoresis has many medical applications. Prototypes that separate cancer cells from healthy cells have been made. Platelets have been separated from whole blood with a DEP-activated cell sorter.

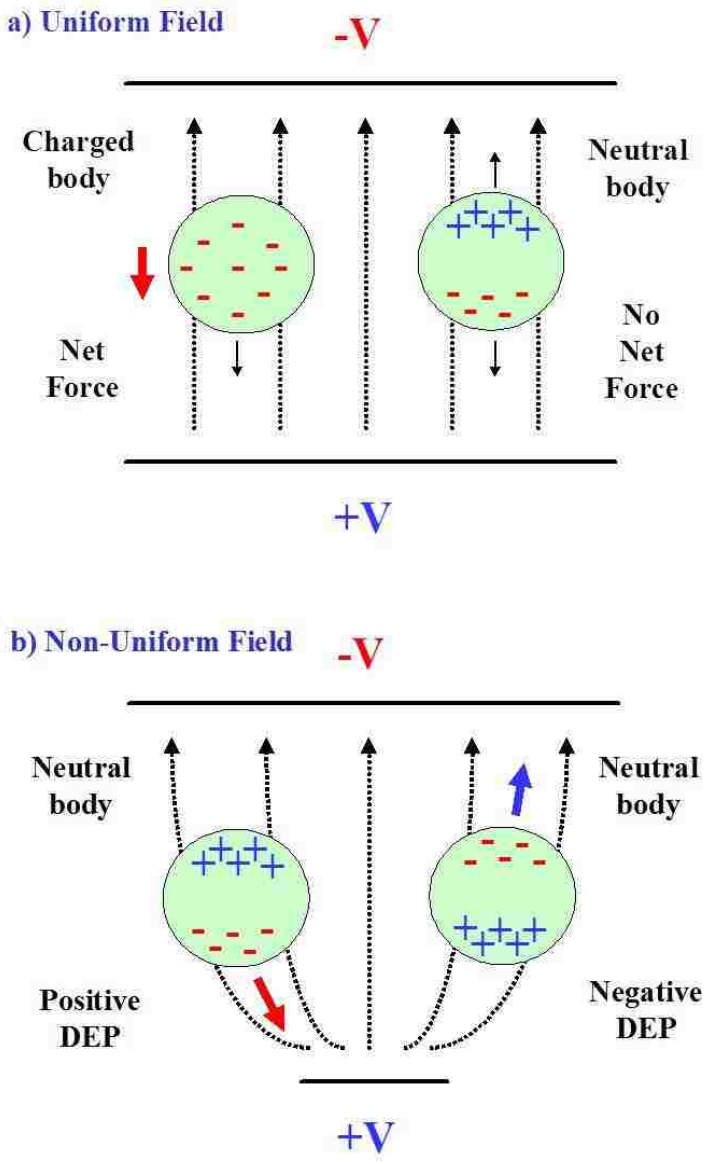

Figure 10 Positive and Negative Dielectrophoresis.

Streaming Potential

Streaming potential and streaming current phenomena are two interrelated electrokinetic phenomena. An electric potential or current originates when

an electrolyte is driven by a pressure gradient through a channel or porous plug with charged walls. The presence of EDL at the solid-liquid interface is the point of origin of these phenomena. The counterions in the diffuse layer of the EDL are transported along with the pressure driven fluid flow. This will cause a potential gradient to be set up in the direction of the flow motion, the magnitude of which will depend upon the rate at which charges are transported by the moving liquid and upon the resistance to the flow of an electric current in the direction opposite to that of the streaming. This potential gradient is known as the streaming potential gradient. The total potential built up in the direction of streaming in this manner is the streaming potential (Lauffer & Gortner, 1939).

From the governing equations in the direction of flow in the fully developed region, the streamwise momentum equation is given by (Conlisk, 2013)

$$\mu \frac{\partial^2 u}{\partial y^2} = \frac{\partial p}{\partial x} - \rho_{el} E_x \tag{2.35}$$

where, ρ_{el} is the volume charge density, E_x is the streamwise component of induced electric field, and u is the velocity composed of pressure-driven and electrically-driven components. The streaming potential corresponds to potential associated with E_x in the above equation.

Consider a channel that is wide and long compared to its height as shown in Figure 11. For sake of simplicity the origin is taken at the center of the channel, so the height is $2h$, and the pressure driven flow is assumed to be fully developed (Conlisk, 2013). By applying following boundary conditions and using equation 2.7, we can solve the governing equation 2.35, to get velocity

$$@\, y = h,\ u = 0 \text{ and } \varphi = \zeta \tag{2.36}$$

$$@\, y = 0,\ \frac{\partial u}{\partial y} = 0 \text{ and } \frac{\partial \varphi}{\partial y} = 0 \tag{2.37}$$

Thus, from equations 2.7,2.35,2.36 and 2.37 we get

$$u(y) = \frac{1}{2\mu}\frac{dP}{dx}(y^2 - h^2) + \frac{\varepsilon}{\mu}(\zeta - \varphi)E_x \tag{2.38}$$

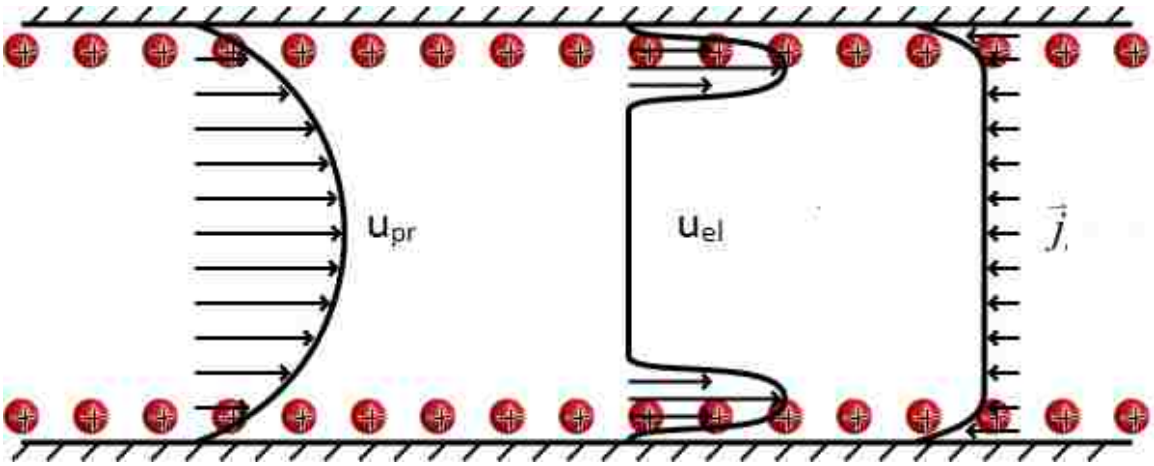

Figure 11 Streaming Potential in a channel (Kirby, 2009).

Current flux is defined by

$$\vec{J} = F\sum_i z_i \vec{N}_i \tag{2.39}$$

where, $\vec{N}_i$ is the species flux given by

$$\vec{N}_i = -D\nabla c_i + c_i\vec{u} - D\frac{ze}{k_B T}c_i\vec{E} \tag{2.40}$$

Here, since convection is dominant, we can neglect concentration gradients. Integrating the streamwise component of current density, we can obtain the total current

$$I = \int_{-h}^{h} J_x dy \tag{2.41}$$

We also know that

$$\sum_i Fz_i c_i = \rho_{el} = -\varepsilon \frac{\partial^2 \varphi}{\partial y^2} \tag{2.42}$$

Substituting for J_x at $I = 0$, from equations 2.39, 2.40 and 2.42 we get

$$\sigma_e E_x \int_{-h}^{h} dy - \varepsilon \int_{-h}^{h} \frac{\partial^2 \varphi}{\partial y^2} u dy = 0 \tag{2.43}$$

where, $\sigma_e = D \frac{Fz_i^{\,2} e}{k_B T} c_i$ is the electrical conductivity of the electrolyte. Now, substituting equation 2.38 in equation 2.43 and solving we get electric field per width of channel

$$E_x = -\frac{\partial \varphi_{sp}}{\partial x} = -2h \frac{\frac{\varepsilon}{\mu} \frac{dp}{dx} \varsigma}{2h\sigma_e + \frac{\varepsilon^2}{\mu} \int_{-h}^{h} (\frac{d\varphi}{dy})^2 dy} \tag{2.44}$$

Under the limit of thin EDL, higher order terms of equation 2.44 can be neglected, giving

$$E_x = -\frac{\partial \varphi_{sp}}{\partial x} = -\frac{\varepsilon}{\mu} \frac{dp}{dx} \frac{\varsigma}{\sigma_e} \tag{2.45}$$

CHAPTER 3

THE POLARIZATION OF A DIFFUSE SOFT PARTICLE SUBJECTED TO AN ALTERNATING CURRENT FIELD

Introduction

There is a strong interest in characterizing electrokinetic properties of colloidal or biocolloidal particles including adsorbed polyelectrolytes (Donath et. al., 1980; Donath et. al., 1986; Starov et. al., 1993(1); Starov et. al., 1993(2)), bacteria (Bos et.al., 1998; de Kerchove et. al., 2005), and environmental colloids like humic substance (Duval et. al., 2005). The aforementioned particles can be categorized as soft particles in which rigid cores are coated with charged polyelectrolytic shells (Cametti, 2011; Dukhin et. al., 2004; Dukhin et. al., 2005; Duval et. al., 2006; Hill et. al., 2004; Hill et. al., 2003(1); Hill et. al., 1993(2); Levine et. al., 1983; Lopez-Garcia et. al., 2003(1); Lopez-Garcia et. al., 2003(2); Lopez-Garcia et. al., 2003(3); Ohshima, 1995; Ohshima, 2000; Ohshima, 2005; Saville, 2000; Sharp, 1985; Wunderlich, 1982). Soft particles can find various applications in nanocomposite (Pyung et. al., 2001), catalysis (Jiang et. al., 2009), sensing (Wu et. al., 2009), self-cleaning materials (Motornov et. al., 2007), and biotechnology (Chanana, 2009).

Since the coated charged polyelectrolytic layer can complicate ions' transport including migration, convection, and diffusion, making the electrokinetic phenomena much complex, theoretical understanding of electrokinetic properties of soft particles under the action of an electric field becomes necessary and important. In fact, sophistical

theoretical models have been developed to study the electrophoretic mobility of soft particles over a broad range of charge densities, coatings, and double layer thicknesses (Duval, 2006; Hill et. al., 2003(1); Hill et. al., 2003(2); Hill et. al., 2005; Ohshima, 1993; Ohshima, 1994; Ohshima, 2000; Saville, 2000).

Compared to extensive investigations on the electrophoretic mobility of soft particles, much less attention has been paid to their electrical polarization in response to an alternating current (AC) electric field (Cametti, 2011). Nowadays dielectrophoresis (DEP) is a promising and popular means to manipulate and control particles in an AC field (Jones, 1995; Lei et. al, 2011; Pohl, 1978; Pethig, 2010; Zhao, 2011). Knowledge of the dipole moment that characterizes the electrical polarization is the key to implement DEP. However, due to intriguing properties of soft particles which lie between rigid particles and porous vesicles (Cametti, 2011), the electrical polarization is not yet completely understood. Again, the charged soft layer complicates ions' transport and makes the interpretation of dielectric behaviors more difficult.

First let us briefly review the dipole moment of bare colloidal particles that has been thoroughly investigated (Lopez-Garcia, 2000; Mangelsdorf, 1997; Zhao, 2009; Zhou, 2005). A charged rigid particle suspended in an electrolyte solution is surrounded by an electric double layer (EDL) (Hunter, 2001; Lyklema, 1995). The imposed electric field drives excess counterions inside the EDL to migrate, resulting in an electro-osmotic flow. Hence migration and convection of excess ions within the EDL along the particle's surface polarize the EDL and change the dipole moment, leading to the high-frequency dispersion (Zhao, 2011). Under the thin double layer limit, migration and convection can be approximated as surface conduction. A simple model termed the Maxwell-Wagner-

O'konski (MWO) theory can be used to calculate the dipole moment induced by the EDL polarization (O'konski, 1960).

It is recognized that the electric field repels ions into the EDL and attracts ions from the EDL at different ends of the particle. This ion-exchange process with the bulk, termed concentration polarization outside the EDL, creates a concentration gradient. As the time scale is larger than the diffusion time or the frequency is lower than the diffusion frequency, bulk diffusion plays a role in determining the dipole moment, creating the low-frequency dispersion. Under the assumptions of the thin quasi-equilibrium EDL and bulk electroneutrality, a theory named the Dukhin-Shilov (DS) model is developed to predict the dipole moment at low frequencies (Dukhin, 1974; Grosse, 1996; Shilov, 1970). For a rigid particle, the high-frequency and low-frequency dispersions fully describe the polarization process.

Similar to their rigid counterpart, the polarization of soft particles shall have both high-frequency and low-frequency dispersions. But the presence of the soft layer complicates the convection and migration inside the EDL. Moreover, excess ions within the soft layer also contribute to the polarization, which may be dominant under certain conditions. Therefore, the impact of the soft layer needs to be examined and understood.

In this manuscript, we will employ a continuum electrokinetic model developed by Duval et al. (Duval et. al., 2006; Duval, 2005; Duval et. al., 2004). This model is based on the Nernst-Planck equation for ion concentrations across the soft layer, Poisson equation for the electric potential, and the Stokes equation that approximates the hydrodynamic impact of polymer chains as a distribution of Stokes resistance centers. The model adopts a diffuse interface to continuously connect the soft layer with the bulk

electrolyte. Within this interfacial zone, the properties gradually change. This model has been successfully implemented to study the electrophoresis of soft particles (Duval et. al., 2006).

Lopez-Garcia et al. studied the dielectric properties of suspensions of charged spherical hard particles enclosed by permeable membranes in an electrolyte solution (Ahualli, 2009). In their work, the focus was on the dielectric spectrum of colloidal suspensions of soft particles and they did not explicitly consider the impact of the characteristics of the soft layer including the Donnan potential, the thickness and the friction coefficient. For example, only two Donnan potentials were investigated and no direct comparisons of these two cases were made. Although Hill et al (Hill et. al., 2003). examined the impact of the Donnan potential on the polarizability of dilute suspensions of spherical colloidal particles with charged coatings, they only investigated the influence of the Donnan potential on the low-frequency limit of the polarization that corresponds to a DC field and did not examine the impact at higher frequencies which is more relevant to DEP techniques. In contrast, here we will provide a full picture of characteristics of the soft layer like the Donnan potential or the soft layer thickness on the polarization of a soft particle over a broad range of frequency. In addition, we carry out a detailed asymptotic analysis on the electrokinetic model and derive simple analytical expressions to compute the dipole moment in the limits of thin double layers and thin soft layers. More specifically, we extend the standard Maxwell-Wagner-O'konski and Dukhin-Shilov theories by accounting for the impact of the soft layer on migration, convection and diffusion. Our approximate formulas can be used to verify and validate numerical

simulations. Finally, we study the dependence of the dipole moment on the double layer thickness, the soft layer thickness and the friction coefficient of the soft layer.

Mathematical Model

An uncharged rigid core of radius a^* and permittivity ε_2^* surrounded by an ion-permeable charged shell with the thickness δ^* is submerged in a symmetric, quiescent electrolyte solution of permittivity ε_1^*. An AC electric field is imposed far from the particle. The imposed electric field is symmetric with respect to the particle's axis and induces the particle to experience an electrophoretic motion, given by $\vec{U}^*(t) = U_0^* e^{i\omega t}$ where U_0^* , the electrophoretic mobility, is not known *a priori* and will be determined during the solution process. Accounting for symmetry, we use a spherical coordinate system (r, θ) with its origin at the particle's center. θ is the angle between the radial direction e_r and the horizontal direction e_z. We fix the origin of the coordinate system at the particle's center. Figure 12 depicts the geometry and the coordinate system. In the following, the superscript * denotes the dimensional form of various variables. Variables without the superscript * are dimensionless. We use the rigid core radius a^* as the length scale; $\frac{R^*T^*}{F^*}$ as the electric potential scale; $\frac{\varepsilon^* R^{*2} T^{*2}}{\mu^* F^2 a^*}$ as the velocity scale; $\frac{a^{*2}}{D_+^*}$ as the time scale; $\frac{\varepsilon^* R^{*2} T^{*2}}{F^2 a^{*2}}$ as the pressure scale; $\frac{\varepsilon^* R^* T^*}{F^* a^*}$ as the electric charge scale.

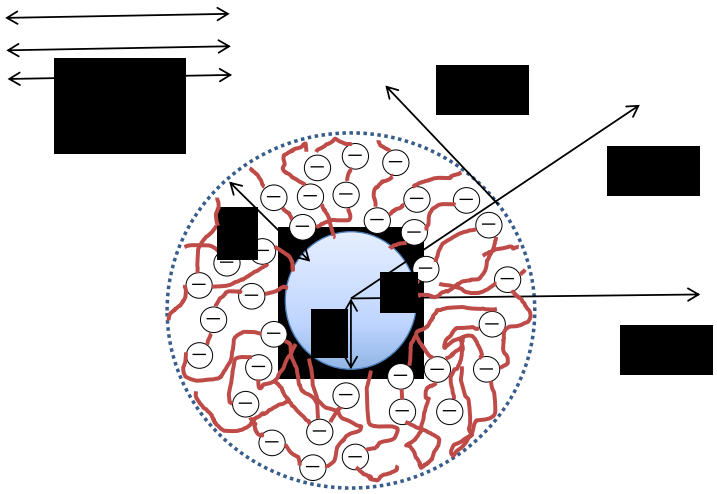

Figure 12 Schematic description of the geometry and the spherical coordinate system.

In the presence of an electric field, excess counterions inside both the soft layer and electric double layer migrate and drag the solvent with them. This fluid motion induces shear forces on the particle and the soft layer surrounding the particle. The resistance provided by the soft layer can be modeled within the framework of the Debye-Beuche model (Debye et. al., 1948).

Because the Reynolds number associated with the electrokinetic flow is small, the fluid flow is modeled with the Stokes equation:

$$-\nabla p - \frac{1}{2\lambda_D^2}(C_+ - C_-)\nabla\varphi_1 + \nabla^2\vec{u} - h(r)k_0\vec{u} = 0 \qquad (3.1)$$

The fluid is incompressible:

$$\nabla \cdot \vec{u} = 0 \qquad (3.2)$$

The electric potential of liquid satisfies the Poisson equation and the particle's electric potential obeys the Laplace equation:

$$\nabla^2\varphi_1 = -\frac{(C_+ - C_- + \rho_{fix}h(r))}{2\lambda_D^2} \tag{3.3}$$

$$\nabla^2\varphi_2 = 0 \tag{3.4}$$

Ionic concentrations are governed by the Nernst-Planck equations:

$$\frac{\partial C_\pm}{\partial t} = -\nabla \bullet \vec{N}_\pm = -\nabla \bullet \left(D_\pm \nabla C_\pm + D_\pm z_\pm C_\pm \nabla\varphi_1 - mC_\pm \vec{u}\right) \tag{3.5}$$

In the above, $\vec{u}$ is the velocity vector; t is time; p is the pressure; C is the ion's concentration; the subscripts (+) and (-) denote, respectively, the cations and the anions; φ is the electric potential; and $E = -\nabla\varphi$ is the electric field. Subscripts 1 and 2 denote the liquid and the rigid bare core, respectively. $\lambda_D = \frac{1}{a^*}\sqrt{\frac{\varepsilon^* R^* T^*}{2F^{*2}C_0^*}}$ is the dimensionless Debye screening length (normalized with the rigid core radius a^*); C_0^* is the solute bulk concentration; R^* is the ideal gas constant; F^* is the Faraday constant; T^* is the temperature; $\rho_{fix} = \frac{\rho_{fix}^*}{F^* C_0^*}$ is the fixed charge density within the soft layer; $m = \frac{\varepsilon_1^* R^{*2} T^{*2}}{\mu^* D_+^* F^{*2}}$ is the cation mobility; μ^* is the solvent viscosity; D_+^* is the cation diffusivity. $k_0 = \left(\frac{a^*}{\gamma_0^*}\right)^2$ is the hydrodynamic friction coefficient where γ_0^* is the hydrodynamic penetration length of the fluid in the soft layer, commonly known as the "softness parameter" (Duval, 2005),

$h(r) = \frac{w}{2}(1 - \tanh(\frac{r-(1+\delta)}{\alpha}))$ is a function of location that remains constant inside the soft layer and is equal to zero outside the soft layer where α is the thickness of the transition layer that is connecting the soft layer to the electrolyte. w is the dimensionless parameter given by

$$w = \frac{2((1+\delta)^3 - 1)}{3\int_1^{\infty}(1 - \tanh(\frac{r-(1+\delta)}{\alpha}))r^2 dr} \tag{3.6}$$

which guarantees that the total charge due to fixed charges inside the soft layer remains constant when varying δ or α. $h(r)$ has been demonstrated to successfully characterize the distribution of the polymer segment within the diffuse layer (Yezek et.al., 2005) and yield reasonable agreements with experimental data for biological and environmental particles (Duval et.al., 2005). Hence we choose $h(r)$ to approximate the continuous interfacial fixed charge density distribution within the soft layer.

The following boundary conditions are imposed. Far from the particle,

$$\varphi_1 = -E_0 r\cos\theta e^{i\omega t},\ C_{\pm} = 1, \text{ and } \vec{u} = -U_0 e^{i\omega t}\vec{e}_z, \text{ at } r \to \infty \tag{3.7}$$

On the rigid surface,

$$\frac{\partial\varphi_1}{\partial n} - \varepsilon_r\frac{\partial\varphi_2}{\partial n} = 0,\ \varphi_1 - \varphi_2 = 0, \text{ and } \vec{n}\bullet\vec{N}_{\pm} = 0 \quad (r = 1) \tag{3.8}$$

In the above, $\varepsilon_r = \varepsilon_2^* / \varepsilon_1^*$ is the relative permittivity, $\vec{n}$ denotes the outer normal vector to the surface, and in our case, $\varepsilon_r = 0.025$.

Perturbation Method

Assuming that the imposed electric field is much smaller than that induced by the fixed charge, a regular perturbation expansion can be used in terms of the applied electric field about the equilibrium EDL:

$$\begin{pmatrix} \varphi \\ C_{\pm} \\ \vec{u} \end{pmatrix} = \begin{pmatrix} \varphi^{(0)} \\ C_{\pm}^{(0)} \\ 0 \end{pmatrix} + \Lambda \mathrm{Re}\left(\begin{pmatrix} \varphi^{(1)} \\ C_{\pm}^{(1)} \\ \vec{u}^{(1)} \end{pmatrix} e^{i\omega t} \right) + 0\left(\Lambda^2\right) \tag{3.9}$$

Where, the symbol *Re* indicates the real part of a complex variable. To determine the particle's electrophoretic mobility U_0, we will set the net force including both hydrodynamic and electrostatic forces to zero.

The zeroth order approximation

Let $\varphi^{(0)}$ and $C_{\pm}^{(0)}$ be, respectively, the equilibrium electric potential and the equilibrium concentrations induced by fixed charges within the soft layer in the absence of an external electric field. Since the zeroth order problem is axisymmetric, the zeroth order variables are only functions of the radial coordinate (r). At equilibrium, the ions' concentrations $C_{\pm}^{(0)}$ obey the Boltzmann distribution:

$$C_{\pm}^{(0)} = e^{\mp\varphi^{(0)}} \tag{3.10}$$

The electric potential $\varphi^{(0)}$ satisfies:

$$\frac{1}{r^2}\frac{d}{dr}\left(r^2 \frac{d\varphi^{(0)}}{dr} \right) = \frac{1}{\lambda_D^2}\left(\sinh(\varphi^{(0)}) - \frac{\rho_{fix}}{2} h(r) \right) \tag{3.11}$$

The boundary conditions are:

$$\frac{d\varphi_1^{(0)}(1)}{dr} = \varphi_1^{(0)}(\infty) = 0 \tag{3.12}$$

The first order approximation

The first order equations are linear in the perturbed quantities. In other words, the dependent-variables oscillate at the forcing frequency. For mathematical convenience, the original problem can be decomposed into two sub problems: (i) the **E** problem consists of the same electric field at infinity as the original problem and zero velocity at infinity and (ii) the **U** problem consists of a zero electric field and a uniform flow field at infinity (O'Brien et. al., 1978).The solutions of the first order problem can be written as the superposition

$$X^{(1)} = (X^{(1)E} + U_0 X^{(1)U}) e^{i\omega t} \tag{3.13}$$

where X represents any of the dependent variables including velocities, electric potential, and ionic concentrations. **E** and **U** denote, respectively, the solutions of the **E** and **U** problems. Substituting series (3.9) into Eqs. (3.1) – (3.55), retaining terms up to $O(\Lambda)$ and replacing the time derivative with $i\omega$, we obtain

$$-\nabla p^{(1)} - \frac{1}{2\lambda_D^2}((C_+^{(1)} - C_-^{(1)})\nabla\varphi_1^{(0)} + (C_+^{(0)} - C_-^{(0)})\nabla\varphi_1^{(1)}) + \nabla^2\vec{u}^{(1)} - h(r)k_0\vec{u}^{(1)} = 0 \tag{3.14}$$

$$\nabla^2\varphi_1^{(1)} = -\frac{(C_+^{(1)} - C_-^{(1)})}{2\lambda_D^2} \tag{3.15}$$

$$\nabla^2\varphi_2^{(1)} = 0 \tag{3.16}$$

and

$$i\omega C_{\pm}^{(1)} = \nabla \bullet \left(D_{\pm} \nabla C_{\pm}^{(1)} + D_{\pm} z_{\pm} (C_{\pm}^{(0)} \nabla \varphi_1^{(1)} + C_{\pm}^{(1)} \nabla \varphi_1^{(0)}) - n C_{\pm}^{(0)} \vec{u}^{(1)} \right) \qquad (3.17)$$

Consider the axisymmetric nature of the problem. Eqs. (14)-(17) can be further simplified to ordinary differential equations (Zhao, 2009), which were solved with the commercial finite element software COMSOL 3.5® (Comsol is a product of Comsol™, Boston). The computational domain is defined as $[0, R]$. Here $R = 10^4$ that is large enough to render the computational results reasonably *R*-independent since a five-fold increase in *R* resulted in variations less than 1%. To resolve the details of the electric double layer and the soft layer, non-uniform elements were applied with a dense mesh concentration next the particle's surface and the elements' size gradually increases as moving away from the surface. We refined mesh a few times to assure that the computational results are mesh-independent.

The dipole moment coefficient

The particle and its adjacent electric double layer perturb the electric field. Far from the particle, the perturbed field appears like a field induced by a dipole, and the electric potential admits the form $E_0(-r + \frac{f}{r^2})\cos\theta$, where the real part of *f* is the dipole coefficient. The dipole coefficient $\mathrm{Re}(f)$ is a function of the Donnan potential (y_d) characterizing the importance of the impact of the fixed charges inside the soft layer ($y_d = \sinh^{-1}\left(\frac{\rho_{fix}}{2}\right)$), the double layer thickness, the soft layer thickness, the friction

coefficient, and the electric field's frequency. Re(f) can be deduced from the behavior of the potential $\varphi^{(1)}$ as a function of r sufficiently far from the particle $(1 << r << R)$.

Surface Conduction (MWO) Model

Often the dipole coefficient of a spherical particle is approximated as (Pohl, 1978)

$$f = \frac{\bar{\varepsilon}_2^* - \bar{\varepsilon}_1^*}{\bar{\varepsilon}_2^* + 2\bar{\varepsilon}_1^*} \tag{3.18}$$

where

$$\bar{\varepsilon}_i^* = \varepsilon_i^* - i\frac{2\pi\sigma_i^*}{\omega^*} \tag{3.19}$$

In the above, $\bar{\varepsilon}_1^*$ and $\bar{\varepsilon}_2^*$ are, respectively, the complex permittivities of the electrolyte and the soft particle; σ_1^* and σ_2^* are, respectively, the conductivities of the electrolyte and the particle. The electrolyte's conductivity is given by $\sigma_1^* = \frac{2F^{*2}D_+^*C_0^*}{R^*T^*}$ (Lyklema, 1995). The particle's effective conductivity is $\sigma_2^* = \sigma_2^{(i)*} + 2\sigma_s^*/a^*$, where $\sigma_2^{(i)*}$ and σ_s^* are, respectively, the intrinsic conductivity of the particle and the surface conduction including both contributions from the soft layer and the double layer.

Here, we assume that $\sigma_2^{(i)*} = 0$ (dielectric core). When the soft layer is thin and the double layer thickness is smaller than the soft layer length ($\delta << 1$ and $\lambda_D/\delta << 1$), we can derive the surface conduction (see Appendix A) as

$$\sigma_s^* = \sigma_1^* \left(\cosh(y_d) - 1 + \frac{m\rho_{fix}^2}{4\lambda_D^2 k_0} \right) \delta^* \tag{3.20}$$

where, y_d is the Donnan potential defined earlier. In the low-frequency limit ($\omega \to 0$), $f = \frac{\sigma_2^* - \sigma_1^*}{\sigma_2^* + 2\sigma_1^*} = \frac{Du - 1}{Du + 2}$ where $Du = \frac{\sigma_2^*}{\sigma_1^*}$ is the Dukhin number, characterizing the importance of the surface conduction.

The Low-frequency (Dukhin-Shilov) Model

It is recognized that under the action of the electric field ions migrate and convect into/from the bulk, inducing a concentration gradient (Dukhin et. al., 1974; Grosse et. al., 1996; Shilov Et. al., 1970). When the frequency is around D_+^* / a^{*2} associated with the diffusion time, ions have enough time to diffuse in response to the concentration polarization. Accordingly, the diffusion changes the dipole coefficient. However, the MWO model does not account for diffusion in the electrolyte solution and cannot capture the behavior of the dipole moment at low frequencies.

To understand the role of the diffusion, Dukhin and Shilov (Dukhin et. al., 1974; Grosse et. al., 1996; Shilov Et. al., 1970), used asymptotic analysis to calculate the dipole coefficient in the limit of thin double layers, $\lambda_D << 1$. In the thin EDL limit, Gross and Shilov[45] outlined a detailed procedure to derive the dipole moment for a rigid spherical particle. Briefly, the bulk concentration and the electric potential in the bulk region obey diffusion equation and Laplace equation, respectively. To solve the above equations, effective boundary conditions outside the EDL are derived by assuming a thin EDL in

local equilibrium (i.e., the chemical potential in the EDL is independent of the radial coordinate). The electric potential and bulk concentration can be solved analytically with the proper boundary conditions.

The presence of the soft layer modifies the effective boundary conditions and we need to incorporate the contribution from the soft layer into the surface conduction. With the proper effective boundary conditions, we can derive the dipole moment of a soft particle under the limits of thin soft layers and thin EDLs. The detailed derivation is given in Appendix B. Here we only present the final expression of the dipole moment:

$$f = A/B \tag{3.21}$$

where

$$A = (1+Wi)(1+W)(2R_+ + 2R_- - 2) + (1+W+Wi)(U_-(2R_+ - 1) + U_+(2R_- - 1)) \tag{3.22}$$

$$B = 2(1+Wi)(1+W)(R_+ + R_- + 2) + (1+W+Wi)(U_-(R_+ + 1) + U_+(R_- + 1)) \tag{3.23}$$

$$R_\pm = \delta(e^{\mp y_d} - 1)\left(1 \mp \frac{m\rho_0}{2\lambda_D^2 k_0}\right) \tag{3.24}$$

$$U_\pm = \delta(e^{\mp y_d} - 1)\left(1 - \frac{m\cosh(y_d)}{\lambda_D^2 k_0}\right) \tag{3.25}$$

$$W = \sqrt{\frac{\omega}{2}} \tag{3.26}$$

At high frequencies ($\omega >> 1$) equation (21) reduces to

$$f = \frac{R_+ + R_- - 1}{R_+ + R_- + 2} = \frac{Du - 1}{Du + 2} \tag{3.27}$$

where $R_+ + R_- = Du$. Not surprisingly, the high-frequency limit of the DS model is equal to the low-frequency limit of the MWO model.

In the low-frequency limit ($\omega \to 0$) equation (21) becomes

$$f = \frac{2R_+(1+U_-) + 2R_-(1+U_+) - (2+U_+ + U_-)}{R_+(2+U_-) + R_-(2+U_+) + (4+U_+ + U_-)} \tag{3.28}$$

Results and discussion

First, we compared our dipole moments (solid line) to the computational results (symbols) reported in Hill et al. (Hill et. al., 2004). Figure 13 plots the dipole coefficient (the real part of *f*) as a function of the frequency where $\lambda_D = 0.096$, $y_d = -1.99$, $\delta = 0.63$, and $k_0 = 816$. The parameters in our model are the same as those in Hill et al. (Hill et. al., 2004). The good agreement is remarkable since our approximation of the structure and permeability of the soft layer is different from that in Hill et al. In other words, the agreement indicates that the impact of the detailed treatment of the soft layer on the dipole moment may be negligible as long as the fundamental characteristics of the soft layer including Donnan potential, the soft layer thickness, and the hydrodynamic friction remain the same. Hill et al. focused on the influence of the polarizability of soft particles on conductivity and dielectric increments of dilute suspensions. In contrast, here we are explicitly interested in the polarization of a single soft particle over a broad range frequency which can find applications in dielectrophoresis.

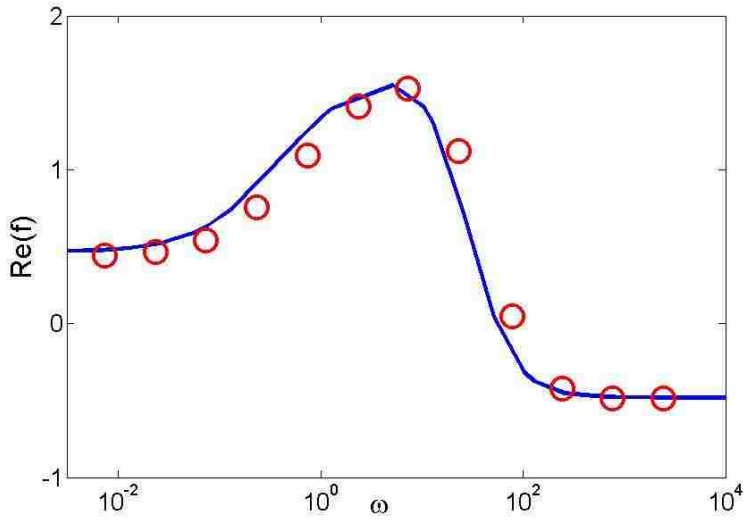

Figure 13 The dipole coefficient *Re(f)* as a function of the frequency ω. The solid line and symbols correspond, respectively, to the dipole coefficient predicted by our model and the one reported in Hill et al. (Hill et. al., 2004).

Figure 14a and 14b depict the dipole coefficient Re(*f*) as a function of the frequency ω for various Donnan potentials and soft layer thicknesses. The solid lines, the dashed lines, and the symbols correspond, respectively, to the predictions from the DS model, the MWO model, and the PNP model.

Figure 14a studies the impact of the Donnan potential on the dipole coefficient when $\lambda_D = 0.01$, $\delta = 0.05$, and $k_0 = 10^6$. The various symbols (in ascending order) correspond, respectively, to $y_d = -2$, $y_d = -4$, and $y_d = -6$. The increase of the Donnan potential (the higher fixed charge density) inside the soft layer leads to a higher concentration of excess mobile ions in the soft layer, yielding to a higher polarization or a

larger Re(*f*). At high frequencies, ions do not have time to respond to the applied electric field. The polarization is dominated by the mismatch of dielectric permittivities of the medium and the particle. Since the dielectric permittivity of the particle is much smaller than that of the electrolyte, the dipole moment is negative. As the frequency decreases, ions have time to migrate and convect. The ions' migration and convection inside the soft layer induce surface conduction. Typically, surface conduction is larger than the bulk conductivity. The dipole moment arises, resulting in the high-frequency dispersion. When the frequency is further decreased around D_+^*/a^{*2}, concentration gradient induced by surface conduction starts to trigger the diffusion process. The dipole moment is dictated by a balance between surface conduction and diffusion. Consider that the direction of diffusion is opposite to that of the surface conduction. The dipole moment decreases as the frequency decreases. When the frequency is much smaller than D_+^*/a^{*2}, the polarization is eventually balanced by the diffusion and surface conduction and the dipole moment is nearly independent of the frequency.

Evidently, the MWO model accounts for surface conduction including migration and convection, captures the high-frequency dispersion, and agrees well with the PNP model at high frequencies. The DS model takes the diffusion into account. Hence it predicts the low-frequency dispersion. Since the DS model is derived under the assumption of electroneutrality that is valid when $\omega^* << D_+^*/\lambda_D^{*2}$ (Shilov et. al., 1970), it is not surprising that the DS model fails at high frequencies. In addition, when deriving the MWO and DS models, only the surface conduction inside the soft layer is taken into account and the contribution from the double layer is neglected. As the Donnan potential

increases, the double layer effect becomes important. Therefore, the MWO and DS models deviate from the PNP model.

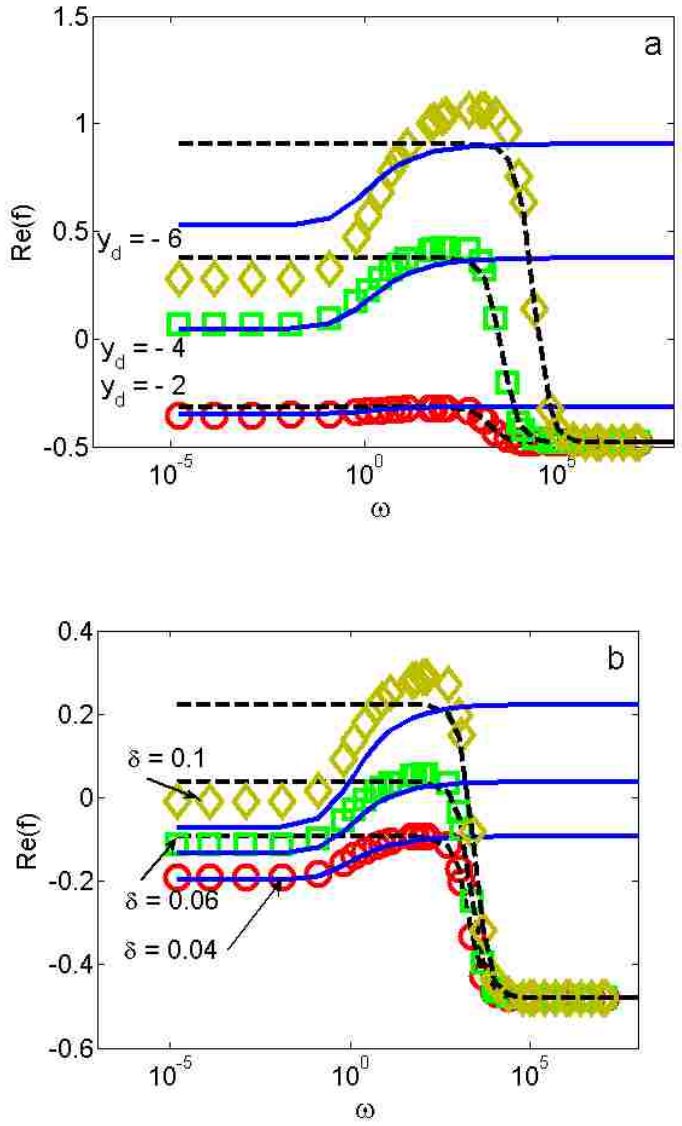

Figure 14 The dipole coefficient Re(*f*) as a function of the frequency ω for (**a**) various Donnan potentials y_d when $\lambda_D = 0.01$, $\delta = 0.05$, and $k_0 = 10^6$, (**b**) various soft layer thicknesses δ when $\lambda_D = 0.01$, $y_D = -3$, and $k_0 = 10^6$.

We also observe that the high-frequency dispersion is shifted to the left as the Donnan potential increases since a higher Donnan potential leads to a larger surface conduction. On the other hand, the Donnan potential has little impact on the low-frequency dispersion, which stays around D_+^* / a^{*2}.

Figure 14b examines the impact of the thickness of the soft layer on the dipole moment when $\lambda_D = 0.01$, $y_D = -3$ and $k_0 = 10^6$. Various symbols correspond, respectively, to $\delta = 0.04$, $\delta = 0.06$ and $\delta = 0.1$. As the thickness of the soft layer increases, the dipole moment increases since there are more excess ions harbored inside the soft layer. Since both MWO and DS models are derived assuming that the thickness of the soft layer is much smaller than the particle's radius, the predictions from the MWO and DS model do not agree well with the PNP model at larger δ.

For an arbitrary double layer thickness and arbitrary Donnan potential, the MWO and DS models are invalid. We have to resort to numerical techniques to solve Eqs. (3.10) - (3.17) to obtain the dipole moment.

Figure 15 plots the dipole coefficient Re(*f*) as a function of the frequency for different double layer thicknesses and Donnan potentials when $\delta = 0.1$ and $k_0 = 10^6$. Interestingly, the dipole moment behaves qualitatively differently at different Donnan potentials. It can be readily explained: on one hand, the double layer extends the charged region further into the bulk. On the other hand, the double layer also sufficiently influences the charge distribution of mobile ions inside the soft layer, in particular, at low Donnan potentials.

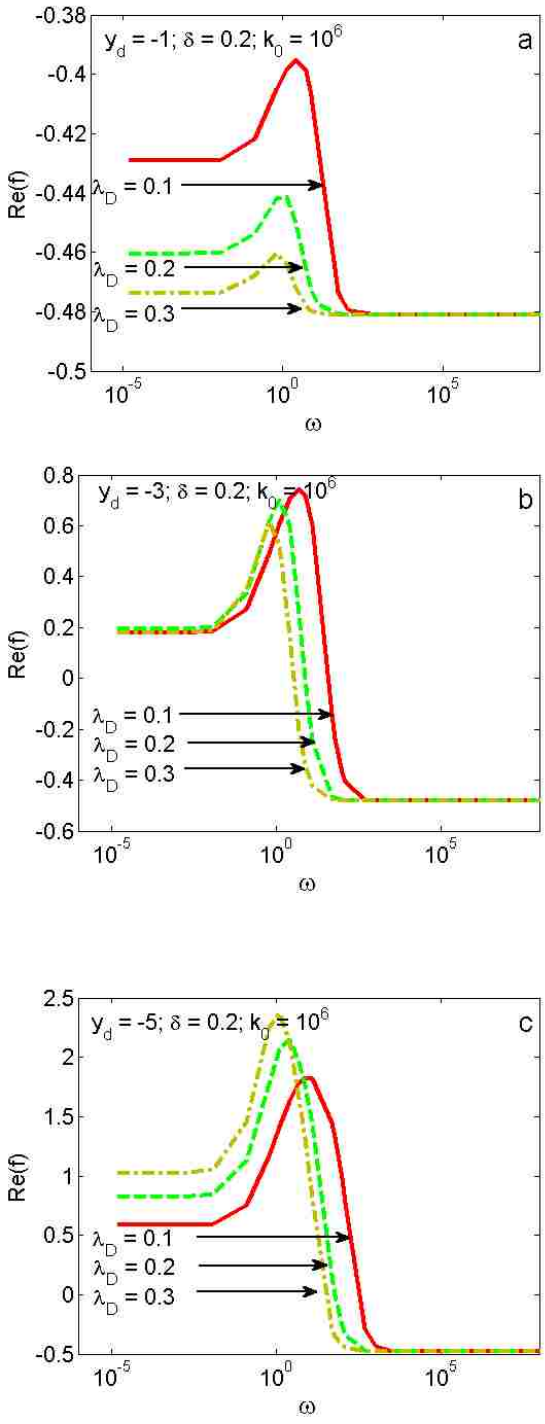

Figure 15 The dipole coefficient Re(*f*) as a function of the frequency ω for various double layer thicknesses and various y_d.

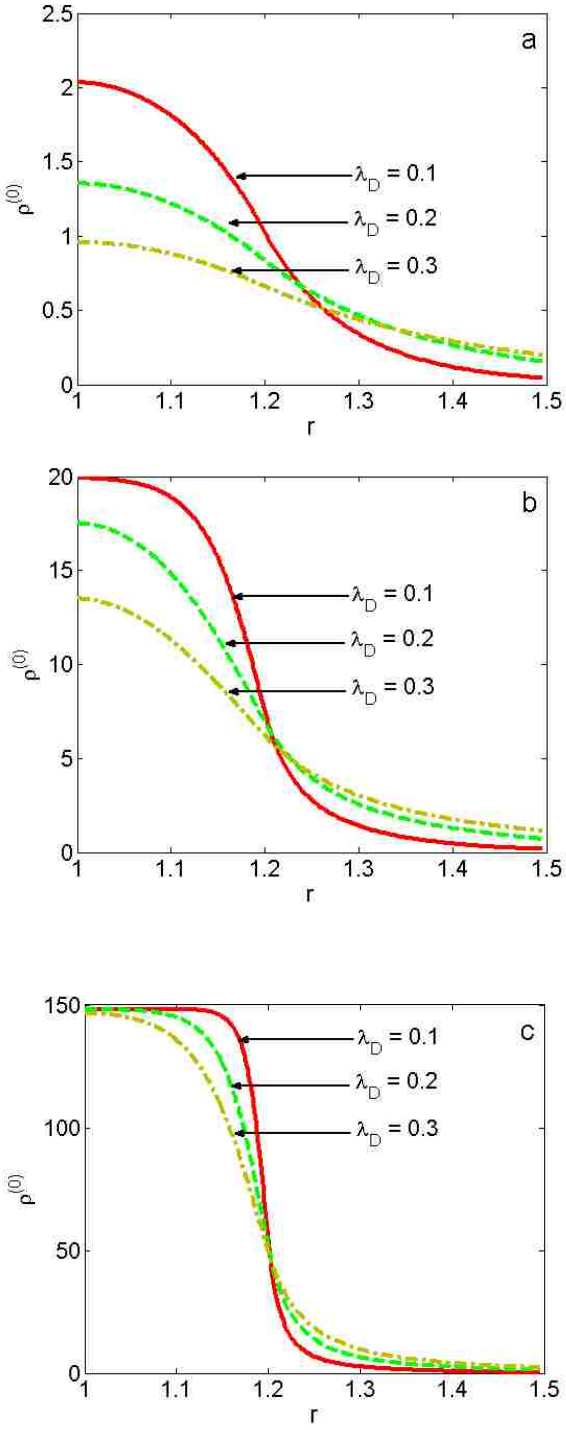

Figure 16 The equilibrium charge distribution of mobile ions across the soft layer for various double layer thicknesses: (**a**) $y_D = -1$, (**b**) $y_D = -3$, (**c**) $y_D = -5$ where $\delta = 0.2$ and $k_0 = 10^6$ into the bulk.

Figure 16a plots the equilibrium charge distribution of mobile ions when $y_D = -1$. Evidently, the charge density of mobile ions inside the soft layer decreases as the double layer thickness increases. Hence, the dipole moment increases as the double layer decreases. However, as the Donnan potential increases, the impact of the double layer on the charge distribution inside the soft layer diminishes and the fixed charges start to dominate the net mobile ions (Figure 16c). Consider that the double layer extends the charged region further.

At large Donnan potentials, the larger the double layer thickness, the higher the dipole moment. Figure 15b shows that around a critical Donnan potential this qualitative transition occurs.

Finally, we examine the influence of the hydrodynamic friction on the dipole moment. Figure 17 plots the dipole moment as a function of the frequency for different k_0 when $\delta = 0.2$, $\lambda_D = 0.1$ and $y_D = -3$. As k_0 increases, the convection inside the soft layer decreases, leading to a reduction of the dipole moment. Meanwhile, with the increase of k_0, the convection becomes weak and its contribution to the dipole moment diminishes. Accordingly, the data of large k_0 collapses onto a single curve.

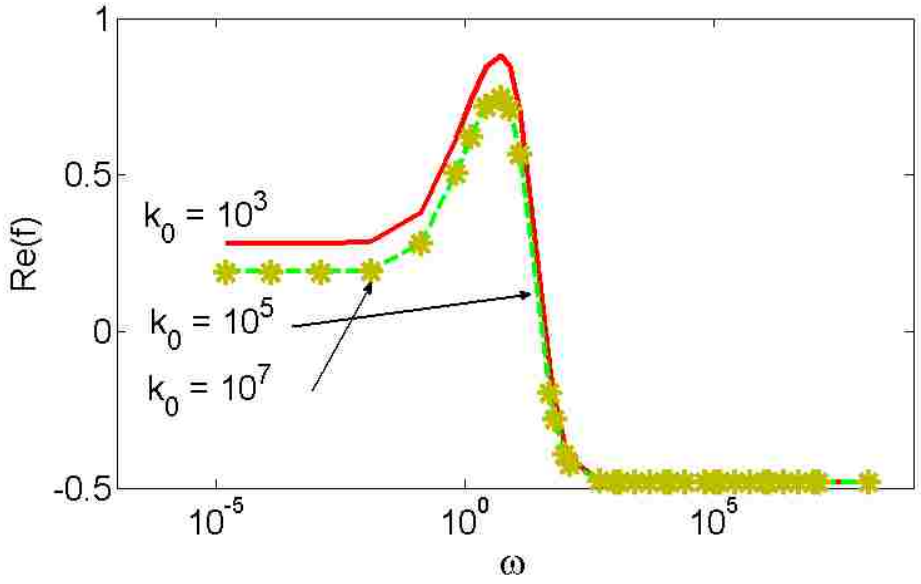

Figure 17 The dipole coefficient Re(*f*) as a function of the frequency ω for different k_0 when $\lambda_D = 0.1$, $y_D = -3$, and $\delta = 0.2$.

Conclusion

In this project, we characterized soft particles as a continuous distribution of charged polymer segments coated on rigid cores and studied the resulting polarization of diffuse spherical soft particles including both the soft layer and double layer under the influence of AC electric fields. The electrostatics and hydrodynamics were solved on the basis of coupled numerical analysis of the nonlinear Poisson-Nernst-Planck and Stokes equations. The dipole moment of a soft particle was computed as a function of its Donnan potential, double layer thickness, hydrodynamic resistance, and soft-layer thickness. In particular, we focused on the impact of the soft layer characteristics on the dipole moment. We found out that at low Donnan potentials, the dipole moment decreases as the

double layer thickness increases. On the contrary, at high Donnan potentials, the dipole moment increases with the increase of the double layer thickness. This qualitative difference is attributed to the impact of the double layer on the charge distribution of mobile ions within the soft layer. In addition, we examined the influence of the hydrodynamic friction coefficient of the soft layer on the polarization as well. As expected, a higher hydrodynamic resistance suppresses the induced electro-osmotic flow inside the soft layer, leading to a reduction of convection. In turn, the dipole moment decreases.

Under the assumption of thin double layers and thin soft layers, we derived the approximate dipole moment expressions for high frequencies accounting for the surface conduction only and low frequencies considering the diffusion. The predictions from our approximations agreed well with the ones predicted by the full model.

Consider that microbes like bacteria, viruses, and yeast cells can be approximated as particles with soft permeable interphases.[54] Quantitative understanding of the polarization of soft particles under the influence of various electrokinetic parameters can make dielectrophoresis a viable technique for sorting, separating, and concentrating microbes, which can find broad applications in biotechnology, food-processing industry, and water-quality monitoring.

CHAPTER 4

THE INFLUENCES OF PARTICLE SIZE AND RESIDUAL CHARGES ON ELECTROSTATIC INTERACTIONS BETWEEN CHARGED COLLOIDAL PARTICLES AT AN OIL-WATER INTERFACE

Introduction

Assembly of colloidal particles can find important technical applications including photonic materials, sensors, optical displays, and electronic devices (Painter et. al., 1999; Vlasov, 2001; Cheng et. al., 2006; Velev and Kaler, 1999; Jiang et. al., 1999). Many methods have been proposed to assemble particles including dielectrophoresis, template-directed sedimentation, depletion, solvent evaporation, spin coating *et al*. (Hayward, 2000; Lumsdon, 2004; Mikhael, 2008; van Blaaderen, 1997; Gates, 1999; Prevo and Velev, 2004 ; Mason and Bibette, 1996; Hobbie, 1998; Denkov, et. al., 1993; Kralchevsky and Denkov, 2001; Jiang and McFarland, 2004; Jiang and McFarland, 2005). One popular method is to self-assemble colloidal particles at the oil-water interface (Bowden et. al., 1999; Bowden, 1997; Grzybowski, 2001; Aubry et. al., 2008; Park and Furst, 2010). The oil-water interface serves as a soft template. Colloidal particles are confined at the interface. For particles with a diameter larger than 10 μm, the gravity deforms the interface locally between the particles (Oettel and Dietrich, 2008) The deformed interface results in attractive lateral capillary forces to self-assemble

particles into monolayer structures. For particles with a diameter smaller than 1 μm, similar clustering is observed as well. However, in this case, the precise origin of attractive forces is still elusive (Bresme and Oettel, 2007). This method is simple, cost-effective and scalable. Because the electrostatic repulsion is the key to self-assembly of colloidal particles at the oil-water interface, fundamental understanding of this repulsion becomes important to make this method be widely implemented.

Electrostatic interactions have been thoroughly theoretically and experimental studied. It is well known that particles pinned at the water-oil interface experiences long-range repulsive dipole-dipole interactions (Pieranski, 1980). Such repulsive interactions are attributed to the asymmetric counter-ion distribution between water and oil phases. In the water phase, the double layer forms near the charged particle surface. Excess counterions inside the double layer screen the electric field generated by the surface charge. In the oil phase, there are mobile ions and the electric field can be extended much further. This asymmetry leads to a dipole normal to the interface. When two particles are close to each other, the double layers overlap and the double layer interactions result in an additional strong short-range repulsive force which decays exponentially as the separation distance increases. To account for both dipole-dipole and double layer interactions, Hurd (Hurd, 1985) computed the linearized Poisson-Boltzmann equation of a single particle and derived a formula to calculate the repulsive force. The simple formula correctly predicts the scaling relationships between the interaction force and the separation distance in both the long ranges and short ranges. However, the predicted magnitude of repulsive force has been found to be significantly lower as compared to experimental measurements.

To understand this discrepancy, Aveyard et. al. (Aveyard et. al., 2002) measured the long-range interactions using laser tweezers method and suggested that the residual charges at oil-particle interface add to the electrostatic repulsion. Later, Masschaele et. al. (Masschaele et. al., 2010), using decane as a non-polar medium and water as polar medium for their experiment, proposed that the finite ion size in the compact or Stern layer of diffuse double layer adds to electrostatic interactions. Oettel *et. al.*(Frydel and Oettel, 2011; Bleibel et. al., 2013) treated particles as point dipoles and computed the electrostatic repulsive force as the dipole-dipole interaction. Similarly, without accounting for steric effects and solvent polarization saturation, the predictions are order-of-magnitude smaller than experimental results. However, consider that the experiments were conducted in DI water. The ion concentration is very low. The steric effect or the finite ion size is not likely significant (Bazant et. al., 2009).

Most theoretical studies treating particles as point dipoles neglected the impact of particle size on the interaction force (Aveyard et. al, 2002; Masschaele et al. 2010; Frydel and Oettel, 2011; Bleibel et. al., 2013).Recognize that the aforementioned long range refers to $d^* / \lambda_D^* >> 10$ where d^* is the particle-particle separation distance and λ_D^* is the double layer thickness. Since λ_D^* is around hundred nanometers, when d^* is around a few μm , d^* / λ_D^* can be larger than 10. However, for micrometer-size colloidal particles, d^* may be comparable to the particle size. In fact, in experiments, $d^* / 2a^* < 10$ where a^* is the particle's radius (Masschaele et. al., 2010) In other words, the influence of the particle size may be important. In addition, the relation in Hurd predicts the dependence of the force on the separation distance for both short and long ranges (Hurd, 1985). But the

force value for a distance in between short and long ranges (i.e. $d^*/\lambda_D^* \sim 10$) is not given by the Hurd's relation.

In contrast, in the present work, we account for the impact of particle size by carrying out three-dimensional simulations of two spherical particles pinned at the oil-water interface via solving the standard Poisson-Nernst-Planck (PNP) model. We also compare the predicted magnitude of the short as well as long range repulsive forces with experimental results of Masschaele *et. al.* (Masschaele et. al., 2010).

Mathematical model

Here we consider two charged spherical particles of radius a^* with a charge density σ^* pinned at the oil-water interface with a contact angle of $\theta^* = 90^0$. Two particles are separated with a distance d^*. The water and oil (decane) have different dielectric permittivities $\varepsilon_r^{(1)}$ and $\varepsilon_r^{(2)}$, respectively. Accounting for the symmetrical nature of interactions between two particles, appropriate axisymmetry and boundary conditions can be applied to significantly simplify the problem. A Cartesian coordinate (*x*, *y*, *z*) with its origin at the center of two particles at the oil-water interface is used to describe the problem, as shown in Figure 18.

To facilitate the analysis, we nondimensionalize the governing equations. We use the radius a^* as the length scale, R^*T^*/F_a^* as the electrical potential scale, C_0^* as the concentration scale, and $\varepsilon_r^{(1)}\varepsilon_0^* R^*T^*/F_a^* a^*$ as the charge scale. Here, C_0^* is the solute bulk concentration; R^* is the ideal gas constant; F_a^* is the Faraday constant; ε_0^* is the permittivity of free space. In the following, to avoid confusion, we use superscript * to

denote the dimensional form of various variables and variables without the superscript * are dimensionless. In addition, superscripts $^{(1),\ (2)}$ denote water and decane medium respectively.

The electric potential of the water satisfies the Poisson equation:

$$\nabla^2 \varphi^{(1)} = -\frac{C_+ - C_-}{2\lambda_D^2} \tag{4.1}$$

In contrast, because the decane is a non-polar medium and contains no ions, the electric potential satisfies the Laplace's equation:

$$\nabla^2 \varphi^{(2)} = 0 \tag{4.2}$$

Ion concentrations in water are described by Nernst-Planck equations:

$$\frac{\partial C_\pm}{\partial t} = \nabla \bullet [-\nabla C_\pm - z_\pm C_\pm \nabla \varphi^{(1)}] \tag{4.3}$$

In the above, φ is the electric potential, $\lambda_D = \frac{1}{a^*}\sqrt{\frac{\varepsilon_r{}^{(1)} \varepsilon_0{}^* R^* T^*}{2F_a{}^{*2} C_0^*}}$ is the thickness of electric double layer, $C_\pm$ is concentration of cations or anions; and $z_\pm$ is the valence number of cations and anions. Here $z_\pm = \pm 1$.

The following boundary conditions are imposed:

$$\begin{aligned} &-\frac{\partial C_\pm}{\partial n} - z_\pm C_\pm \frac{\partial \varphi^{(1)}}{\partial n} = 0 \\ &\varepsilon_r{}^{(1)} \frac{\partial \varphi}{\partial n} = \varepsilon_r{}^{(2)} \frac{\partial \varphi}{\partial n} \quad \text{, at the oil-water interface } (z=0); \\ &\varphi^{(1)} = \varphi^{(2)} \end{aligned} \tag{4.4}$$

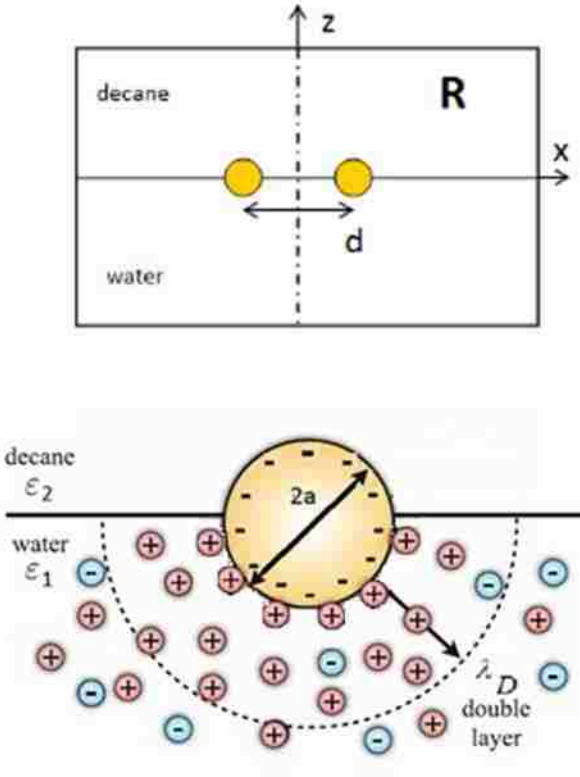

Figure 18 Schematic illustration of 3D model for a particle trapped at Decane-Water interface.

$$-\frac{\partial C_{\pm}}{\partial n} - z_{\pm} C_{\pm} \frac{\partial \varphi^{(1)}}{\partial n} = 0 \,(z < 0)$$
$$\frac{\partial \varphi}{\partial x} = 0 \,(z < 0) \qquad \text{at the center } (x=0); \qquad (4.5)$$
$$\frac{\partial \varphi}{\partial x} = 0 \,(z > 0)$$

$$\varphi^{(1)} = 0 \,(z < 0)$$
$$C_{\pm} = 1 \,(z < 0) \quad \text{at the far field } (z = \pm R, x = R); \qquad (4.6)$$
$$\varphi^{(2)} = 0 \,(z > 0)$$

and

$$
\begin{aligned}
&-\varepsilon^{(1)}\frac{\partial\varphi^{(1)}}{\partial n}=\sigma\,(z<0)\\
&-\frac{\partial C_{\pm}}{\partial n}-z_{\pm}C_{\pm}\frac{\partial\varphi^{(1)}}{\partial n}=0\,(z<0)\ \text{ on the particle interface.}\\
&-\varepsilon^{(2)}\frac{\partial\varphi^{(2)}}{\partial n}=\sigma\,(z>0)
\end{aligned}
\tag{4.7}
$$

In the above, σ is the surface charge density. The ionic flux across the oil-water interface is assumed to be zero, since most of the simple electrolytes are composed of hydrophilic ions that dissolve easily in water rather than in oil, making ion transport difficult across the oil-water interface (Verdes et. al, 2004; Kornyshev et. al., 2002).

Accounting for the symmetry, only the *x*-component of the electrostatic force is not equal to zero. To compute it, we integrate the Maxwell stress tensor over the entire surface of the particle.

$$F_x=\int(\vec{E}\vec{E}-\frac{1}{2}(\vec{E}\cdot\vec{E})I)\cdot\hat{n}_x dA. \tag{4.8}$$

The model is solved with the commercial finite-element software 4.3b COMSOL®. Eqs. (4.1)-(4.7) were solved using the generalized minimal residual method. The computational domain consisted of a finite domain $0<x<R$ and $-R<z<R$ where *R=50*. It is considered to be sufficiently large. To assure that the solutions are independent of the domain size *R*, we further increase *R* by a factor of 1.5 and the discrepancies between these two domains were less than 0.1%. In order to resolve the detailed structures of the electric double layer, non-uniform elements were used with dense meshes with the maximum element size of 0.004 (approximate twenty elements) concentrated next to the particle's surface inside the electric double layer. The maximum

element size in the bulk is set to be 0.08 near the domain edges. The meshes were refined a few times as well to guarantee that the results are mesh-independent.

Results and Discussion

When a particle is trapped at the decane-water interface, an electric double layer (EDL) forms near the charged surface of the particle on the water side by attracting counterions and repelling coions, but not on the decane side since the decane contains no ions. The presence of EDL on the water side can effectively screen the electric field induced by the surface charge. Figure 19 plots the contours of the electric potential around the particle at the decane-water interface. Evidently, on the water side, the electric potential quickly decreases to zero away from the particle. In contrast, on the decane side, the electric field extends much further into the bulk.

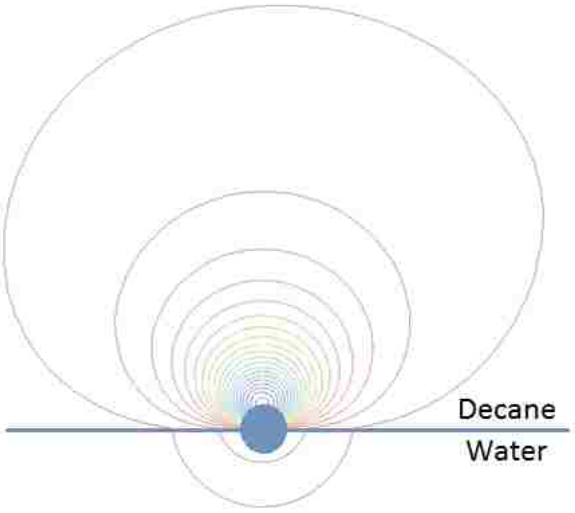

Figure 19 Potential gradient for a particle trapped at Decane-Water interface, XZ view.

It is well known that at long ranges, the repulsive force between two particles behaves like the dipole-dipole repulsion. It was predicted that the interaction force decays as $\sim d^{-4}$. Here the long range typically refers to $d/\lambda_D >> 10$ (Aveyard et. al., 2002; Masschaele et.al., 2010). To verify our computational algorithm, we first compute the electrostatic force as a function of the center-to-center distance between two particles. Figure 20 plots the electrostatic force as a function of d/λ_D when $\lambda_D = 0.2; \sigma = -0.3$. The symbols represent the computed force values and the solid line represents the best power-law fit $F_x \sim d^{-4.04}$. Our numerical results agreed well with the dipole-dipole interactions.

For short ranges, when the particles are very close to each other, the EDLs of two particles overlap, resulting in the double-layer interaction. It is recognized that the double-layer interaction is dominate at short ranges, yielding to an exponential scaling relationship (Hurd, 1985; Aveyard et. al., 2002; Masschaele et.al., 2010).

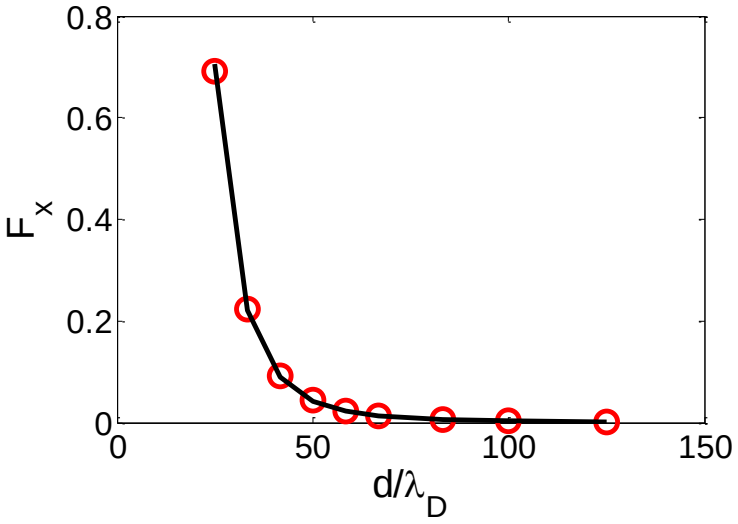

Figure 20 Variation of long range horizontal repulsive force as a function of center-to-center particle distance as $F_x \sim d^{-4.04}$ at $\lambda_D = 0.2; \sigma = -0.3$.

Figure 21 plots the short-range electrostatic force as a function of $(d-2)/\lambda_D$ when $\lambda_D = 0.2; \sigma = -0.3$. Symbols and the solid black line represent the computed force values and the best exponential fit, $F_x \sim e^{-0.48d}$, respectively. Once again, the good fitting further verifies our computational algorithm.

Next we examine the effect of the surface charge density on the electrostatic interaction force. Figure 22 plots the repulsive force as a function of the surface charge density when $\lambda_D = 0.2$. The symbols and the solid lines correspond, respectively to the computed force and best polynomial fit. Circles and diamonds correspond to the forces at $d = 2.05$ (short range) and $d = 6.67$ (long range), respectively. The quadratic relationship between the predicted force and the surface charge density at all ranges can be readily explained: the repulsive force is electrostatic in nature, which is directly correlated with the surface charges of two neighboring particles.

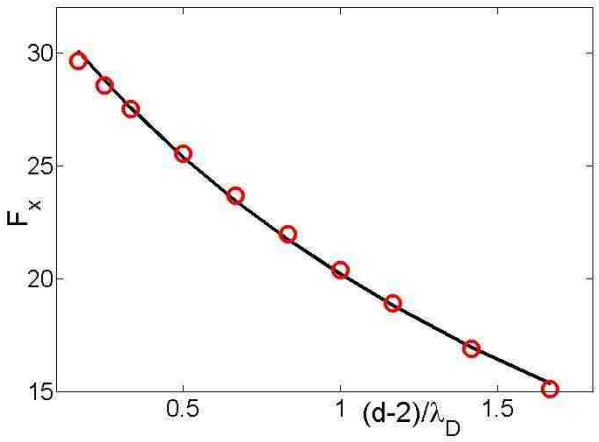

Figure 21 Variation of short range horizontal repulsive force as a function of center-to-center particle distance as $F_x \sim e^{-0.48d}$ at $\lambda_D = 0.2; \sigma = -0.3$.

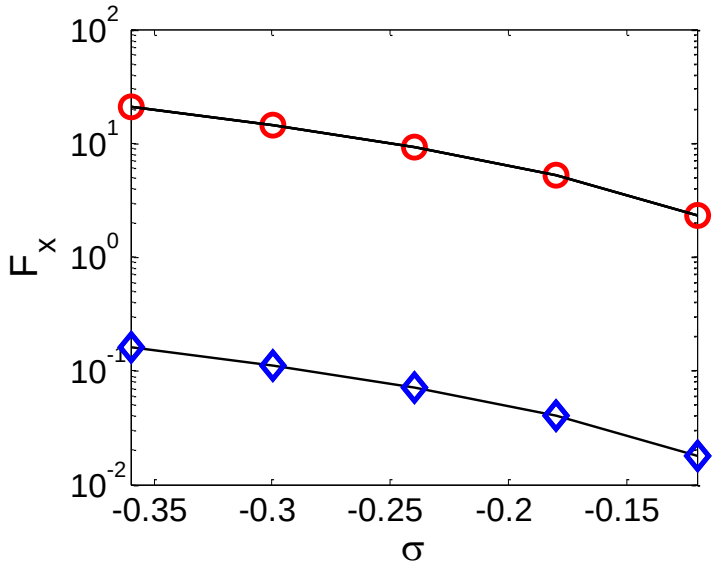

Figure 22 Horizontal force as a function of surface charge density for $\lambda_D = 0.2$; circles represent force at $d = 2.05$; and squares at $d = 16.67$. In both cases force varies as $F_x \sim \sigma^2$.

Finally, we examine whether the standard PNP model is adequate to describe the particle-particle electrostatic interaction at the oil-water interface. Recently Masschaele *et al.* used different methods to measure the interaction forces among polystyrene particles at the decane-water interface including optical tweezers, macroscopic rheological measurements and strain fluctuations (Masschaele et.al., 2010). Measurements are consistent among different techniques. Figure 23 depicts the experimentally measured dimensional forces (symbols) by Masschaele *et al.* (Masschaele et.al., 2010). and our computed dimensional forces (lines) from the PNP model as a function of the dimensional distance d^*. Two sets of numerical simulations with and without the residual charge at the particle-oil interface were carried out for the same conditions as in the experiments. In the absence of the residual surface charge, we fit the surface charge density $\sigma^{*(1)}$ at the particle-water interface by matching the force value at $d^* = 6.31\mu m$.

The corresponding zeta potential is computed to be around -76 mV which is within the general range of experimentally measured zeta potentials for polystyrene particles (Ma et. al.). Figure 23, suggests that despite the good agreement at short ranges, without considering the residual charge, the predictions (the dashed line) are order-of-magnitude smaller than the experimental results at long ranges. In contrast, by assuming a small residual surface charge $\sigma^{*(2)}$, the predicted forces (the solid line) quantitatively agree with experiments over a large range of distances including both small and large separation distances. The favorable agreement at long ranges strongly suggests that there is the possible presence of residual charges in the oil phase. Indeed, recent experiments also indicate that particles have residual charges in the non-polar-medium, which are consistent with our findings here (Aveyard et. al., 2002; Law et. al., 2013; Law et. al., 2011; Ma and Dai, 2009; Hsu et. al., 2005; Briscoe and Horn, 2002; Aveyard et. al., 2000).

Aveyard *et al.* (Aveyard et. al., 2002; Aveyard et. al., 2000) derived an expression for the charged-dipole interaction force between particles assuming that there are residual charges at the particle-oil interface:

$$F_x^* = \frac{3a_d^* k_b T^*}{r^{*4}} \tag{4.9}$$

where k_b is the Boltzmann constant and a_d^* is the energy scale of the interaction:

$$a_d^* = \frac{9\pi a^{*6}\sigma^{*(2)2}}{2\varepsilon_0^*\varepsilon_r^{(2)}k_b T^*}. \tag{4.10}$$

By inserting our fitted $\sigma^{*(2)} = -1.41\,\mu C/m^2$ into Eq. (10), we can compute $a_d = 5.35\times10^{-15}\,\mathrm{m}^3$. With a_d, Eq. (9) gives the force value around $4\times10^{-4}\,\mathrm{pN}$ at $d^* = 20\,\mu\mathrm{m}$, which is an order-of-magnitude smaller than the experimental data or the simulation value. Since Eq. (4.9) assumes point dipoles and does not explicitly take into account the impact of particle size on the particle-particle interaction, this discrepancy suggests that the impact of particle size is not negligible even at long ranges.

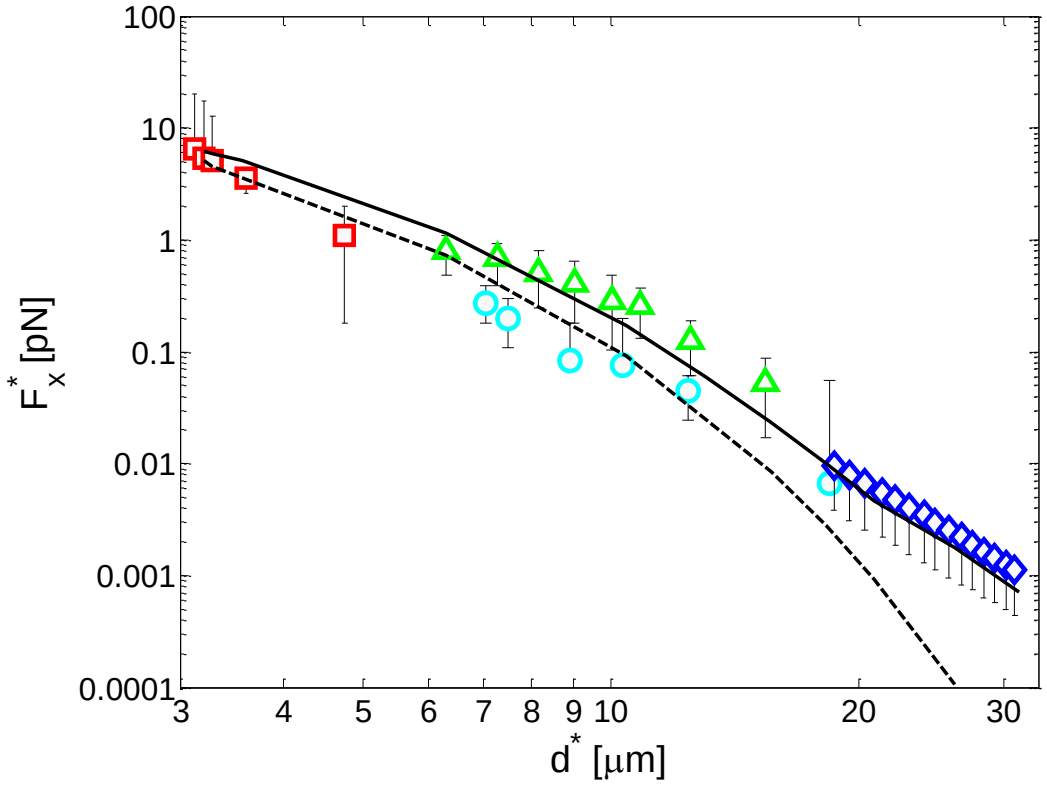

Figure 23 Comparison of the predicted force (lines) and the measured force (symbols). The dashed line represents the force values evaluated at $\lambda_D^* = 300\,\mathrm{nm}$; $a^* = 1.55\,\mu\mathrm{m}$; $\sigma^{*(1)} = -70.4\,\mu C/m^2$ and $\sigma^{*(2)} = 0\,\mu C/m^2$. The solid line represents the force values evaluated at $\sigma^{*(1)} = -70.4\,\mu C/m^2$ and $\sigma^{*(2)} = -1.41\,\mu C/m^2$.

Conclusion

To assemble particles at the oil-water interface, knowledge of the electrostatic repulsive force is important to control and manipulate particles at liquid-liquid interfaces. To understand the particle-particle electrostatic interactions, often the dipole-dipole approximation neglecting particle size was used to interpret experimental data. However, the dipole-dipole approximation is only capable of qualitatively explaining the long-range interaction. When particles are close to each other, the geometry of the particle plays an important role in determining the interaction force since the particle can disturb the electric field distribution in the oil side which is not screened by the double layer. One would expect that the dipole-dipole approximation without considering the impact of the particle's geometry fails.

Here we numerically solved the standard Poisson-Nernst-Planck equations for the interaction of two spherical particles. The model accounts for the impact of particle size. Our model successfully predicted the fourth-power scaling relation at long ranges and the exponential relation at short ranges. In addition, since our model does not have any assumption on the ranges, our model can bridge the short and long ranges and compute the force at any given particle-particle distance.

By assuming that the particle in the oil phase has residual charges, our model compared favorably with experimental data. The good agreements with experiments indicated that the standard PNP model adequately describes particle-particle electrostatic interactions without a need to stipulate the presence of additional physics like steric effects or solvent polarization saturation.

CHAPTER 5

CHARACTERIZATION OF STREAMING POTENTIAL IN A CAPILLARY DUE TO DROP DEFORMATION IN A TWO PHASE FLOW USING PHASE FIELD METHOD AND ADAPTIVE MESHING

Introduction

Streaming potentials are generated when fluid flows past a charged surface. Convection of electric charges within the charge cloud adjacent to the surface leads to a current; if there is no external return path for the current, a potential is established and current returns *via* conduction through the fluid. This phenomenon is well described in Chapter 2. Streaming Potential is generally well understood for single phase flows, for which there is a linear relationship between the pressure drop and the electrical potential difference generated by fluid motion (Lac & Sherwood, 2009). However, streaming potentials generated by multiphase flow are less understood (Morgan *et al.*, 1989; Antraygues & Aubert, 1993). Such flows are of importance in soil, in which the pore space is filled by an air/water mixture, and in petroleum reservoirs (saturated by oil/water/gas mixtures). Practical applications include the detection of water approaching a production well (Wurmstich & Morgan 1994; Jackson *et al.* 2005), and the generation of electrokinetic signals as seismic waves pass a gas/liquid interface.

Theoretical analysis of the streaming potential, generated by a bubble or drop flowing in a fluid-filled capillary for a closely fitting rigid sphere (Sherwood, 2007; Sherwood, 2008), and generated by a drop of viscosity $\mu^{(2)}$ moves along the centerline of a capillary filled by a second fluid of viscosity $\mu^{(1)}$ (Lac & Sherwood, 2009), has been performed. The latter represents an idealized two-phase flow in a porous medium. The presence of the drop is known to modify the pressure difference necessary to maintain a given flow rate, or equivalently, the flow rate driven by a constant pressure difference (Olbricht,1996). Similarly, the drop affects the streaming potential, since both the convective current in the electric double layer and the overall electrical resistances of the capillary are modified by the presence of the drop. Thus, to develop such sensors, it becomes imperative to quantify the influence of a dispersed phase on the relationship between pressure drop and streaming potential.

For the sake of simplicity, we consider the case of a liquid-liquid phase ie, oil-droplet-in-water, so that electric currents are present only in the bulk and the surface of the drop is uncharged. The EDL at the wall of the capillary is assumed to be thin compared to the radius of the capillary and to the width of the gap between the drop and the capillary wall. This result in smaller Hartmann number, in the absence of magnetic field, given as $Ha = L\sqrt{\frac{\sigma}{\mu}}$ where, σ is the conductivity of bulk medium (Lac & Sherwood, 2009). It means that, the electric potential induced by the flow generates negligibly small electrohydrodynamic flows in return, compared to the pressure-driven flow. This simplifying assumption enables decoupling of the hydrodynamics and the

electrokinetics. Hence it is very convenient to solve the flow field first, and then determine the induced streaming potential.

To solve for the flow field, it is necessary to understand the interfacial parameters affecting deformation, if any, of the drop. In other words, the evolution of interface in response to shear rate of the flow, has to be characterized, as this transformation will affect the flow field in the bulk. Flows of gas-liquid or liquid-liquid mixed phases are familiar from many macroscopic systems. The fluid-dynamical response is commonly characterized successfully in terms of the Reynolds and Capillary numbers of the flow.

In general, the mathematical treatment of such moving boundary (evolving interface, in our case) problems is complicated by the fact that the position of the interface is not known a priori. Rather it evolves according to the flow within both fluid phases. A conceptually straightforward method for handling moving boundaries is to keep track of the motion of material points residing on the interface. Numerically, this may be realized by using a moving grid with grid points moving either according to the local fluid velocity or a mesh velocity. This Lagrangian approach is often known as interface tracking (Yue et.al., 2006). Difficulties arise, however, when interfacial deformation becomes severe as to cause mesh entanglement. An alternative to interface tracking is to compute the fluid flow of both components on a fixed Eulerian grid, with the interface being determined or reconstructed at each time step by using a scalar indicator function. Examples of this class of methods are the volume-of-fluid (VoF) method, the level-set method and the phase-field method. In recent years, the phase-field model has gained popularity in simulating two-phase flows of immiscible fluids (Yue et.al., 2006). In this framework, the interface between two immiscible fluids is treated as

a thin mixing layer across which physical properties vary steeply but continuously. The property and evolution of the interfacial layer is governed by a phase-field variable ϕ that obeys a Cahn–Hilliard type of convection-diffusion equation. This circumvents the task of directly tracking the interface, and produces the correct interfacial tension from the mixing energy density at the interface.

Two factors drive the evolution of ϕ: flow and diffusion, which can be described by

$$\frac{\partial \phi}{\partial t} + u \cdot \nabla \phi = \gamma \nabla^2 G \tag{5.1}$$

where, γ is the mobility and G is the chemical potential given as

$$G = \lambda \left[-\nabla^2 \phi + \frac{\phi(\phi - 1)}{\varepsilon_t^2} \right] \tag{5.2}$$

where, λ is the mixing energy density and ε_t is the interface thickness.

The advantages and limitations of the phase-field method, in relationship to other interface-capturing methods, have been discussed before (Feng et.al. 2005). The feasibility of a diffuse-interface approximation for two-phase flows with practically sharp interfaces rests on the fact that the bulk components are identified by ϕ = ±1 and the interface is well defined at ϕ = 0. Since ϕ takes on constant values in the bulk of each component, this further implies conservation of mass for each component provided that the interfacial layer is thin. Thus, the difficulty that requires special attention in level-set and volume-of-fluid methods appears to be nonexistent for the phase-field method. The

greatest challenge of this approach is in resolving the sharp gradients at the interface. This is achieved by using an efficient adaptive meshing scheme governed by the phase-field variable. The finite-element scheme easily accommodates complex flow geometry and the adaptive meshing makes it possible to simulate two-phase systems effectively and efficiently (Zhou, 2008). This work, specifically tries to develop understanding of flow field variations and associated streaming potential change based on changing interfacial tension, for two different drop sizes by using Phase-field model with adaptive mesh refinement.

Mathematical Model

Here we consider a spherical oil droplet of radius a^*, introduced in a stream of water flowing inside a capillary of length, L^* and radius, r^*. The flow is fully developed laminar. Accounting for the symmetrical nature of the geometry, appropriate axisymmetry and boundary conditions can be applied to simplify the problem. A cylindrical coordinate (*r, z*) with its origin at (*r=0, z=0*) is used to describe the problem, as shown in Figure 24. In the following, to avoid confusion, we use superscript * to denote the dimensional form of various variables and variables without the superscript * are dimensionless. In addition, superscripts $^{(1),\ (2)}$ denote water and oil medium respectively.

We nondimensionalize the governing equations, using capillary radius r^* as the length scale, $t^* u_0^{*(1)} / r^*$ as the time scale, $u_0^{*(1)}$ as the velocity scale, ε_t^* / r^* as interface

thickness scale, $p^* r^* / \mu^{*(1)} {u_0}^{*(1)}$ as pressure scale, $\lambda^* / \mu^{*(1)} {u_0}^{*(1)} r^*$ as the force scale, $R^* T^* / Fa^*$ as the potential scale, $Fa^{*2} C_0^* r^{*2} / R^* T^* \varepsilon^{*(1)}$ as the bulk conductivity scale and $\chi^* \mu^*$ as the mobility scale. Here, ${u_0}^*$ is the average velocity at the inlet; p^* is the pressure; μ^* is the viscosity; ε_t^* is the capillary width; λ^* is the mixing energy density, χ^* is the mobility tuning parameter, R^* is the universal gas constant, Fa^* is the Faraday's constant, T^* is the ambient temperature, and ε^* is the absolute permittivity of the medium.

For a horizontal cylinder, in the absence of external force the NS equation becomes:

$$\mathrm{Re}\left(\frac{\partial u}{\partial t} + u \cdot \nabla u\right) = -\nabla p + \nabla^2 u + G \nabla \phi \tag{5.3}$$

where, $\mathrm{Re} = \dfrac{\rho^{*(1)} {u_0}^* L^*}{\mu^{*(1)}}$ is the Reynolds number; ϕ is the phase-field variable; and $G\nabla\phi$ is the surface tension force, in the absence of free energy, $\dfrac{\partial f}{\partial \phi}$. Here $G = \dfrac{1}{Ca} \dfrac{3}{2\sqrt{2}} \varepsilon_t \left[-\nabla^2 \phi + \dfrac{\phi(\phi - 1)}{\varepsilon_t^2} \right]$ is the chemical potential, $Ca = \mu^{*(1)} {u_0}^* / {\sigma_{st}}^*$ is the Capillary number and ${\sigma_{st}}^* = \dfrac{2\sqrt{2}}{3} \dfrac{\lambda^*}{\varepsilon_t^*}$ is the surface tension coefficient. The Re number is very low due to smaller length scales and velocities and hence, nonlinearity can be ignored.

The Phase-field equation is given as:

$$\frac{\partial \phi}{\partial t} + u \cdot \nabla \phi = \chi \lambda \nabla^2 \psi \,. \tag{5.4}$$

where, ψ is the phase-field help variable. In the absence of free energy it is given by:

$$\psi = -\varepsilon_t{}^2 \nabla^2 \phi + \phi\left(\phi^2 - 1\right). \tag{5.5}$$

The electric potential of the water satisfies the Poisson equation:

$$\nabla^2 \varphi^{(1)} = \frac{\sinh V}{\lambda_D^2} \,. \tag{5.6}$$

Oil is a non-polar medium and contains no ions, the electric potential satisfies the Laplace's equation:

$$\nabla^2 \varphi^{(2)} = 0 \,. \tag{5.7}$$

The streaming potential, a function of bulk fluid velocity, volume charge density ρ_v and bulk conductivity σ_e, is given as:

$$V_{strm} = \frac{\int_0^r u \rho_v dA}{\sigma_e} \tag{5.8}$$

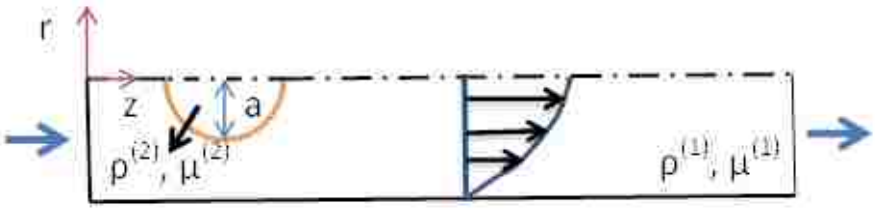

Figure 24 Schematic illustration of 2D axisymmetric model for a oil drop, in a bulk of water, at the centerline of capillary, in a fully developed laminar flow.

The following boundary conditions are imposed:

$$u = 0, \text{ at the walls} \left(r = \pm 1\right) ; \tag{5.9}$$

$$\frac{du}{dr} = 0, \text{ at the centerline} \left(r = 0\right) ; \tag{5.10}$$

$$v = 0; \frac{du}{dz} = 0, \text{ at} \left(z = 0; z = 10\right); \tag{5.11}$$

$$V = \varsigma, \text{ at } \left(r = \pm 1\right); \tag{5.12}$$

$$V = 0, \text{ at } \left(r = a\right); \tag{5.13}$$

Eqs. (5.1)-(5.13) are solved by the commercial finite-element software COMSOL®. The mesh was refined a few times as well to guarantee that the results are mesh-independent.

Results and Discussion

When viscous drops of one fluid are suspended in a second viscous fluid, that is caused to shear, the drops will deform, and, if the local shear rate is sufficiently large, will break into two or more fragments. The degree and rate of deformation, is controlled by the Capillary number of the flow, which gives relative effect of viscous forces versus surface tension.

As the simplest model**,** we have a neutrally buoyant oil drop, which undergoes deformation when introduced in fully developed laminar flow in a capillary carrying water. The ratio of viscosities of oil drop and water is 8. The neutral buoyancy places the drop in the centerline of the capillary and is propelled forward. The shear rate associated with fully developed flow profile deforms the drop. Although, deformed drop shapes can be complicated, it is well known, that the fully developed shear rate of the flow will deform the drop at the forward end giving it a 'bullet' shape, which would vary based on the surface tension at the liquid-liquid interface (Guido &. Perziosi, 2010).

As $Ca \to 0$, the interfacial forces dominate the viscous forces, and the drop retains its spherical shape. As a consequence of reversibility of Stokes equation, the drop would not cross channel streamlines, so only steady motion parallel to the capillary walls results (Griggs et.al., 2007). Figure 25, below shows drop deformation and motion for $Ca = 0.01$ and $\mathrm{Re} = 10^{-5}$. The drop retains its spherical shape and moves along the centerline of the channel, thus qualitatively validating our model.

Figure 25 Drop deformation at $Ca = 0.01,\ t = 5$ and $\mathrm{Re} = 10^{-5}$.

The transient migration of highly deformable drop, ($Ca = 1$), which was initially undeformed and placed at the centerline of the capillary, is shown in Figure 26. The drop initially elongates in the direction of the Poiseuille flow and eventually obtains a steady shape that is compact and symmetric about the channel centerline. This type of dynamic behavior for drop migration is observed for a wide range of Capillary numbers, as shown in Figure 26.

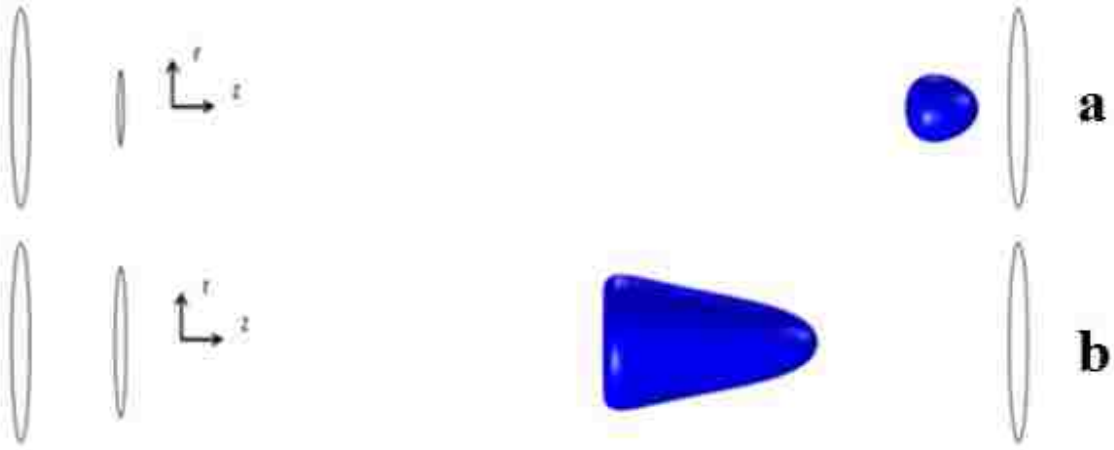

Figure 26 Drop deformation at $t = 5$, $Ca = 1$ and $\mathrm{Re} = 10^{-5}$ (a) $a = 0.375$ (b) $a = 0.75$.

A quick literature survey reveals (Griggs et. al.,2007), that over a wide range of initial conditions, drops move away from the channel walls, towards the channel center,

and obtain a steady position with the drop center in the channel midplane, regardless of the initial placement, size, or Capillary number.

Computed translational velocities for nearly spherical drops are given in Figure 27 for two different drop sizes. The velocities of the drops decrease with increasing drop size. The small drops tend to move with the Poiseuille flow rather than lag behind it.

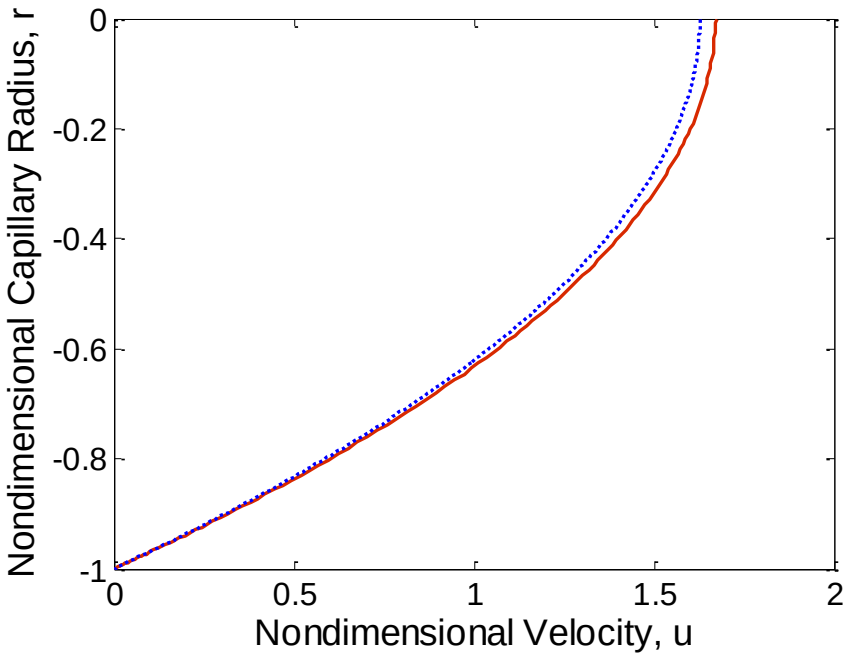

Figure 27 Velocity profile at, $t = 5$, $Ca = 1$ and $\mathrm{Re} = 10^{-5}$ for $a = 0.375$ (solid line) and $a = 0.75$ (dot line).

Figure 28 gives trends for the longitudinal velocities as the drop travels down the channel for nearly spherical and highly deformable drops of same size. For deformable drops, in the initial phase, a decrease in the longitudinal velocity is observed (dash line) and can be attributed to the onset of shape distortion, which increases the drop resistance

to the flow. Following this initial phase of deformation, the longitudinal velocity increases, owing to the streamlined shape adopted by the drops and become stable for maximum deformation.

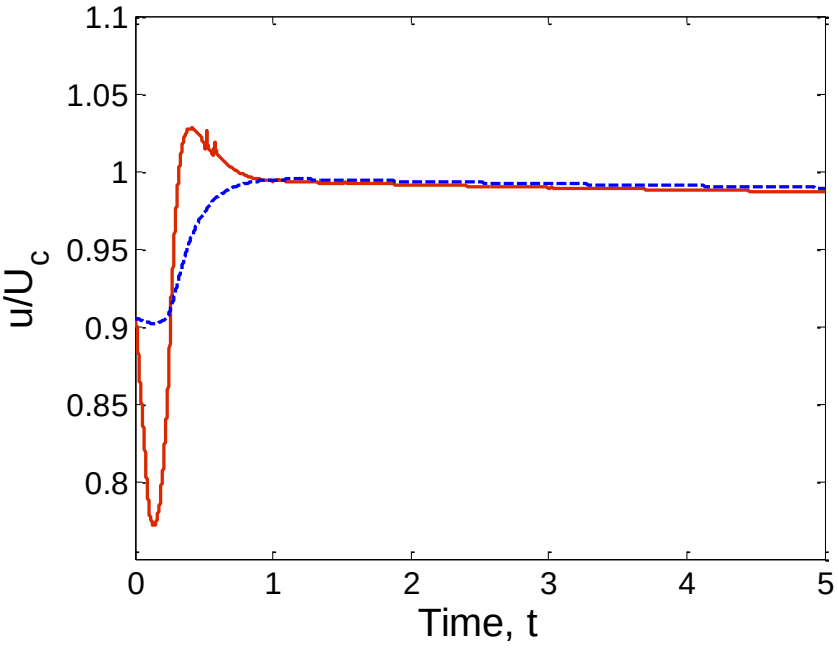

Figure 28 Longitudinal velocity at drop center for, $a = 0.375$ and $\mathrm{Re} = 10^{-5}$ at $Ca = 0.01$ (Solid line), $Ca = 1$ (dash line). U_c is the centerline velocity of unperturbed flow.

Conversely, decrease in longitudinal velocity in the initial phase for a nearly spherical drop (solid line) is relatively higher owing to higher surface tension and resistance to deformation. Following that the drop velocity increase sharply to gain equilibrium with bulk velocity indicating a balance between surface tension force and shear rate after which the drop velocity becomes stable.

Streaming Potentials, evaluated as a function of velocity flow field, volume charge density and electrical conductivity of the electrolyte, given by Eqn. 5.8, are shown in Figure 29. The Streaming Potential V_{strm} increases with increasing drop size and shows the same qualitative pattern for the case of highly deformable drop, $Ca = 1$, irrespective of the drop size. Variation in streaming potential closely correlates to the changes in drop velocity. For deformable drops, the onset of shape distortion increases the drop resistance to the flow. This decreases drop velocity and increases streaming potential. After that, the drop velocity increases, reducing streaming potential which later, achieves a stable value when drop velocity becomes stable.

Conclusion

To develop a two-phase flow sensor, knowledge of the electrokinetics is important to get precision measurements. To understand the streaming potential and/or streaming current phenomena interactions, it becomes necessary to evaluate changes in the bulk flow which in turn is dependent on the variations in two-phase flow. Electrokinetic phenomena while dependent on the flow field can be decoupled from flow field changes due to smaller electric Hartmann numbers.

Here, we numerically solved the Navier-Stokes and Phase field equations along with Poisson's and Laplace equations under the limit of thin EDL, to characterize oil drop deformation and associated streaming potential, respectively.

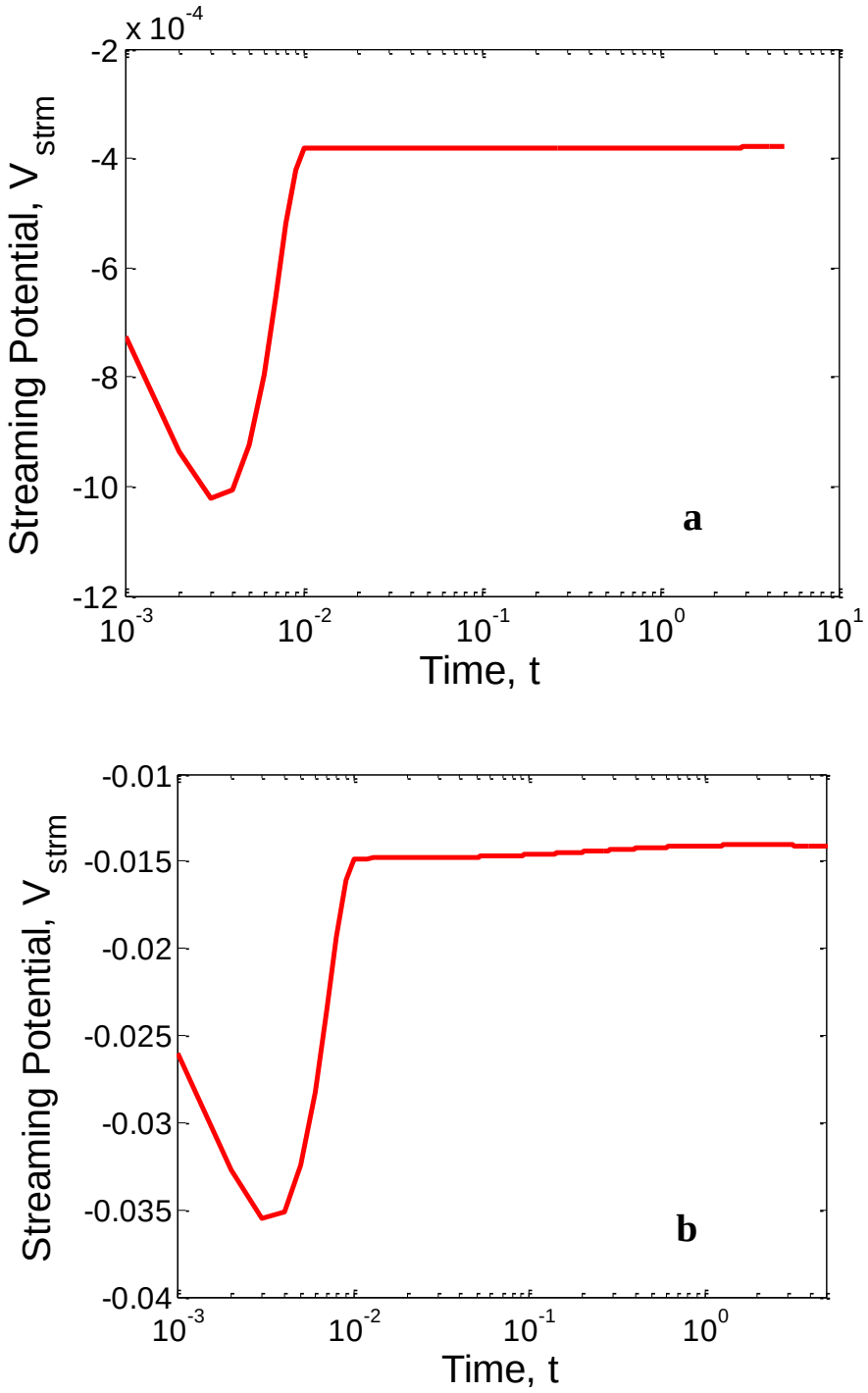

Figure 29 Streaming potential across the capillary, $Ca = 1$ and $\mathrm{Re} = 10^{-5}$ for (a) $a = 0.375$; (b) $a = 0.75$

The Phase field method with adaptive meshing predicts the interfacial tension at the liquid-liquid interface for a wide range of Capillary numbers with good accuracy. The results compare well qualitatively with Griggs et. al. Velocity profile for nearly spherical oil drops, taken at the vertical centerline of the drop, remains qualitatively same for different drop sizes compared with unperturbed fully developed laminar flow. Longitudinal velocity of a deformable oil drop is qualitatively different at different capillary numbers during the initial phase. As expected, drop with lower Capillary number provides more resistance to the flow reducing its own velocity significantly as compared to the drops with higher capillary numbers. Later, the drop experiences sudden increase in velocity with onset of deformation. The rate of increase is qualitatively similar for a wide range of capillary numbers.

Streaming Potentials for deformable oil drops are qualitative similar for different drop sizes. A doubling of the drop size increases magnitude of streaming potential approximately by a factor of 30. As expected, the streaming potential closely tracks the drop velocity. It increases with decrease in drop velocity and vice-versa and reaches a stable value, when drop velocity stabilizes. This variation can be easily be measured, indicating that streaming potential phenomena can potentially be applied to develop sensors to detect and study two phase and multiphase flows.

CHAPTER 6

SUMMARY AND CONCLUSIONS

This study aims to increase understanding of complex electrokinetic phenomena with applications to microfluidic systems. In that regard three cases, with applications in diverse fields as Lab-on-Chip technology, colloidal assembly and petrophysical sensing are considered. The electrokinetic behavior is modeled using standard Poisson-Nernst-Planck model to simulate electric double layer polarization.

Polarization of spherical soft particle, characterized as particle having charged segments attached to the rigid core, under the influence of AC electric field shows surprising findings. The impact of detailed treatment of charged soft layer is negligible if the defining parameters of the soft layers remain same. On the other hand, this study has quantified the polarization of soft particle over wide range of frequencies which can find applications in dielectrophoresis.

Finite volume of the particles, trapped at oil-water interface and presence of residual surface charges at the oil-particle interface, plays major role in the electrostatic interactions of charged particles over a wide range of interparticle separations. The predicted repulsion agrees remarkably well with the experimental results. This helps in quantifying electrokinetic behavior at any given interparticle separation without stipulating additional physics.

Characterization of deformation of oil drop, in a fully developed steady laminar flow, within a flowing bulk of water rests heavily on the characteristics of liquid-liquid interface. As expected, at $Ca << 1$, the drop almost retains its spherical shape while for $Ca = 1$, the drop deforms due to shear stress. The degree of deformation increases with increasing capillary number. These findings can help quantify the flow field distortion and influence on the streaming potential phenomena.

Future Recommendations

Quantifying various electrokinetic phenomena is a complex task especially due multiscale nature of the phenomena. Simulating a 3D model of a domain in which the gradient zone is of a magnitude lower by an order of one or two, becomes computationally intensive and time-consuming.

Simulation of electrostatic interactions between charged particles at oil-water interface under the limit of thin EDL and Evaluation of buoyancy effects on electrostatic interactions of particles at oil-water interface, would provide detailed analysis directly applicable to colloidal assembly. Similarly, simulation of 3D model of a two-phase flow sensor, which includes quantitative validation with experimental data and parametric studies influencing streaming potential would be a major step towards developing predictive models.

Appendix A

In Appendix A, we derive the approximate form of the surface conduction used in calculating the dipole moment in the MWO model in the limit of thin soft layers ($\delta << 1$) and thin double layers ($\lambda_D / \delta << 1$). When $\lambda_D / \delta << 1$, the electric potential inside the soft layer is equal to the Donnan potential y_D. Based on Eq. (14), the velocities outside the double layer within the soft layer become:

$$\vec{u}^{(1)} = \frac{\rho_{fix}}{2\lambda_D^2 k_0} \nabla \varphi_1^{(1)} . \tag{A1}$$

With Eq. (A1), we can derive the dimensionless surface conduction or Dukhin number for a flat soft layer under the limit of thin double layers. Consider a uniform field $E_1 = -\nabla \varphi_1^{(1)}$ applied parallel to the surface. The field drives an ionic surface current j_s through the soft layer, and the surface conduction σ_s is defined as

$$\sigma_s E_1 = \int_0^\infty (j_s - j_b) dy . \tag{A2}$$

In the above, $j_b = \sigma_1 E_1$ is the bulk current outside the soft layer and j_s is given by $N_+ - N_-$ where

$$N_\pm = e^{\mp y_d} (\pm E_1 - m\vec{u}^{(1)}) . \tag{A3}$$

Substituting (A3) into (A2) yields

$$\sigma_s = \sigma_1 \left(\left(\cosh(y_d) - 1 \right) + \frac{m\rho_{fix}^2}{4\lambda_D^2 k_0} \right) \delta . \tag{A4}$$

Appendix B

In Appendix B, we extended the Dukhin and Shilov's asymptotic analysis (Dukhin et. al., 1974; Grosse et. al., 1996; Shilov Et. al., 1970) to compute the dipole coefficient of a soft particle in the limits of thin double layers and thin soft layers. When the applied frequency $\omega^* << D_+^* / \lambda_D^{*2}$,the bulk electrolyte is close to electroneutrality and satisfies

$$i\omega C^{(1)} = \nabla^2 C^{(1)}, \tag{B1}$$

where $C^{(1)} = \frac{C_+^{(1)} + C_-^{(+)}}{2}$. Due to neutrality, the electric potential obeys the Laplace equation:

$$\nabla^2 \varphi_1^{(1)} = 0. \tag{B2}$$

The solution of Eq. (B1) and B(2) can be integrated:

$$C^{(1)} = K_c \frac{e^{-(1+i)W(r-1)}}{r^2} \frac{1+(1+i)Wr}{1+W+iW} \cos\theta, \tag{B3}$$

and

$$\varphi_1^{(1)} = \left(-r + \frac{f}{r^2} \right) \cos\theta. \tag{B4}$$

In the above, $W = \sqrt{\omega/2}$. To determine K_c and *f*, we need to derive effective boundary conditions. We assume that the bulk is at local equilibrium with the soft layer to derive the ion conservation equations in terms of the actual and far field variables, respectively.

Then we can integrate the difference of two equations over the soft layer to obtain the boundary conditions:

$$\left.\frac{\partial \mu_{\pm}^{(1)}}{\partial r}\right|_{r=1} = \pm 2R_{\pm}\varphi_1^{(1)}(1) + 2U_{\pm}C^{(1)}(1), \qquad \text{(B5)}$$

where $\mu_{\pm}^{(1)} = C^{(1)} \pm \varphi_1^{(1)}$ is the perturbed chemical potential. $R_{\pm}$ and $U_{\pm}$ are given in the main text. The detailed procedure to derive (B5) can be found in Grosse and Shilov (Grosse et. al., 1996). Since Fixman demonstrated that the explicit temporal variation of ion concentration under the action of an AC electric field inside the double layer is negligible when the frequency is smaller than $\omega^* << D_+^* / \lambda_D^{*2}$ (Fixman, 1980) , Eq. (B5) does not account for the explicit temporal change of ion concentration inside the soft layer which has been considered by Shilov and Dukhin.

BIBLIOGRAPHY

Ahualli, S., Jiménez, M. L., Carrique, F., & Delgado, A. V. (2009). AC electrokinetics of concentrated suspensions of soft particles. *Langmuir*, *25*(4), 1986-1997.

Antraygues, P., & Aubert, M. (1993). Self potential generated by two-phase flow in a porous medium: Experimental study and volcanological applications.*Journal of Geophysical Research: Solid Earth (1978–2012)*, *98*(B12), 22273-22281.

Aubry, N., Singh, P., Janjua, M., & Nudurupati, S. (2008). Micro-and nanoparticles self-assembly for virtually defect-free, adjustable monolayers. *Proceedings of the National Academy of Sciences*, *105*(10), 3711-3714.

Aveyard, R., Clint, J. H., Nees, D., & Paunov, V. N. (2000). Compression and structure of monolayers of charged latex particles at air/water and octane/water interfaces. *Langmuir*, *16*(4), 1969-1979.

Aveyard, R.; Binks, B.P.; Clint, J.H.; Fletcher, P.D.I.; Horozov, T.S.; Neumann, B.; Paunov, V.N.; Annesley, J.; Botchway, S.W.; Nees, D.; Parker, A.W.; Ward, A.D.; Burgess, A.N. (2002). Measurement of long-range repulsive forces between charged particles at an decane-water interface. *Physical review letters 88.24*: 246102.

Bazant, M. Z., Kilic, M. S., Storey, B. D., & Ajdari, A. (2009). Towards an understanding of induced-charge electrokinetics at large applied voltages in concentrated solutions. *Advances in colloid and interface science*, *152*(1), 48-88.

Bleibel, J., Domínguez, A., & Oettel, M. (2013). Colloidal particles at fluid interfaces: Effective interactions, dynamics and a gravitation–like instability. *The European Physical Journal Special Topics*, *222*(11), 3071-3087.

Bos, R., van der Mei, H. C., & Busscher, H. J. (1998). Soft-particle'analysis of the electrophoretic mobility of a fibrillated and non-fibrillated oral streptococcal strain: Streptococcus salivarius. *Biophysical chemistry*, *74*(3), 251-255.

Bowden, N., Choi, I. S., Grzybowski, B. A., & Whitesides, G. M. (1999). Mesoscale self- assembly of hexagonal plates using lateral capillary forces: synthesis using the "capillary bond". *Journal of the American Chemical Society*,*121*(23), 5373-5391.

Bresme, F., & Oettel, M. (2007). Nanoparticles at fluid interfaces. *Journal of Physics: Condensed Matter*, *19*(41), 413101.

Bruus, H. (2008). Theoretical Microfluidics. Vol. 18. Oxford University Press.

Cametti, C. (2011). Dielectric properties of soft-particles in aqueous solutions. *Soft Matter*, *7*(12), 5494-5506.

Chanana, M., Jahn, S., Georgieva, R., Lutz, J. F., Bäumler, H., & Wang, D. (2009). Fabrication of colloidal stable, thermosensitive, and biocompatible magnetite nanoparticles and study of their reversible agglomeration in aqueous milieu. *Chemistry of Materials*, *21*(9), 1906-1914.

Chang, H. C., & Yeo, L. Y. (2010). *Electrokinetically driven microfluidics and nanofluidics* (pp. 39-40). Cambridge, UK:: Cambridge University Press.

Cheng, W., Wang, J., Jonas, U., Fytas, G., & Stefanou, N. (2006). Observation and tuning of hypersonic bandgaps in colloidal crystals. *Nature Materials*, *5*(10), 830-836.

Conlisk, A. T. (2012). *Essentials of micro-and nanofluidics: with applications to the biological and chemical sciences*. Cambridge University Press.

de Kerchove, A. J., & Elimelech, M. (2005). Relevance of electrokinetic theory for "soft" particles to bacterial cells: implications for bacterial adhesion. *Langmuir*, *21*(14), 6462-6472.

Debye, P., & Bueche, A. M. (2004). Intrinsic viscosity, diffusion, and sedimentation rate of polymers in solution. *The Journal of Chemical Physics*,*16*(6), 573-579.

Denkov, N.D., Velev, O. D., Kralchevsky, P. A., Ivanov, I. B., Yoshimura, H. & Nagayama, K. (1993). Two Dimensional Crystallization. *Nature, 361*, 26.

Dimaki, M., & Bøggild, P. (2004). Dielectrophoresis of carbon nanotubes using microelectrodes: a numerical study. *Nanotechnology*, *15*(8), 1095.

Donath, E., & Pastushenko, V. (1980). 308-Electrophoretic study of cell surface properties theory and experimental applicability. *Bioelectrochemistry and Bioenergetics*, *7*(1), 31-40.

Donath, E., & Voigt, A. (1986). Streaming current and streaming potential on structured surfaces. *Journal of colloid and interface science*, *109*(1), 122-139.

Dukhin, S. S. & Shilov, V. N. (1974). *Dielectric Phenomena & the Double Layer in Disperse Systems & Polyelectrolytes*; New York, NY, Wiley.

Dukhin, S. S., Zimmermann, R., & Werner, C. (2004). Intrinsic charge and Donnan potentials of grafted polyelectrolyte layers determined by surface conductivity data. *Journal of colloid and interface science*, *274*(1), 309-318.

Dukhin, S. S., Zimmermann, R., & Werner, C. (2005). Electrokinetic phenomena at grafted polyelectrolyte layers. *Journal of colloid and interface science*, *286*(2), 761-773.

Duval, J. F. (2005). Electrokinetics of diffuse soft interfaces. 2. Analysis based on the nonlinear Poisson-Boltzmann equation. *Langmuir*, *21*(8), 3247-3258.

Duval, J. F., & Gaboriaud, F. (2010). Progress in electrohydrodynamics of soft microbial particle interphases. *Current Opinion in Colloid & Interface Science*,*15*(3), 184-195.

Duval, J. F., & Ohshima, H. (2006). Electrophoresis of diffuse soft particles.*Langmuir*, *22*(8),3533-3546.

Duval, J. F., & van Leeuwen, H. P. (2004). Electrokinetics of diffuse soft interfaces. 1. Limit of low Donnan potentials. *Langmuir*, *20*(23), 10324-10336.

Duval, J. F., Busscher, H. J., van de Belt-Gritter, B., van der Mei, H. C., & Norde, W. (2005). Analysis of the interfacial properties of fibrillated and nonfibrillated oral streptococcal strains from electrophoretic mobility and titration measurements:

Evidence for the shortcomings of the'classical soft-particle approach'. *Langmuir*, *21*(24), 11268-11282.

Duval, J. F., Wilkinson, K. J., Van Leeuwen, H. P., & Buffle, J. (2005). Humic substances are soft and permeable: evidence from their electrophoretic mobilities. *Environmental science & technology*, *39*(17), 6435-6445.

Feng, J. J., Liu, C., Shen, J., & Yue, P. (2005). An energetic variational formulation with phase field methods for interfacial dynamics of complex fluids: advantages and challenges. In *Modeling of soft matter* (pp. 1-26). Springer New York.

Feynman, R. P., Leighton, R. B., & Sands, M. (2013). *The Feynman Lectures on Physics, Desktop Edition Volume I* (Vol. 1). Basic Books.

Fixman, M. (2008). Charged macromolecules in external fields. I. The sphere. *The Journal of Chemical Physics*, *72*(9), 5177-5186.

Fox, R. W., McDonald, A. T., & Pritchard, P. J. (2006). *Introduction to fluid mechanics*. Hoboken: Wiley.

Frydel, D., & Oettel, M. (2011). Charged particles at fluid interfaces as a probe into structural details of a double layer. *Physical Chemistry Chemical Physics*,*13*(9), 4109-4118.

Ghosal, S. (2004). Fluid mechanics of electroosmotic flow and its effect on band broadening in capillary electrophoresis. *Electrophoresis*, *25*(2), 214-228.

Griggs, A. J., Zinchenko, A. Z., & Davis, R. H. (2007). Low-Reynolds-number motion of a deformable drop between two parallel plane walls. *International journal of multiphase flow*, *33*(2), 182-206.

Grosse, C.; Shilov, V. N. Theory of the low-frequency electrorotation of polystyrene particles in electrolyte solution *J. Phys. Chem.* 1996, *100*, 1771-1778.

Grzybowski, B. A., Bowden, N., Arias, F., Yang, H., & Whitesides, G. M. (2001). Modeling of menisci and capillary forces from the millimeter to the micrometer size range. *The Journal of Physical Chemistry B*, *105*(2), 404-412.

Guido, S., & Preziosi, V. (2010). Droplet deformation under confined Poiseuille flow. *Advances in colloid and interface science*, *161*(1), 89-101.

Hayward, R. C., Saville, D. A., & Aksay, I. A. (2000). Electrophoretic assembly of colloidal crystals with optically tunable micropatterns. *Nature*, *404*(6773), 56-59.

Helmholtz, H. V. (1853). Ueber einige Gesetze der Vertheilung elektrischer Ströme in körperlichen Leitern mit Anwendung auf die thierisch-elektrischen Versuche. *Annalen der Physik*, *165*(6), 211-233.

Herczyński, A. (2013). Bound charges and currents. *American Journal of Physics*, *81*(3), 202-205.

Hill, R. J. (2004). Hydrodynamics and electrokinetics of spherical liposomes with coatings of terminally anchored poly (ethylene glycol): numerically exact

electrokinetics with self-consistent mean-field polymer. *Physical Review E*,*70*(5), 051406.

Hill, R. J., & Saville, D. A. (2005). 'Exact'solutions of the full electrokinetic model for soft spherical colloids: Electrophoretic mobility. *Colloids and Surfaces A: Physicochemical and Engineering Aspects*, *267*(1), 31-49.

Hill, R. J., Saville, D. A., & Russel, W. B. (2003). Electrophoresis of spherical polymer-coated colloidal particles. *Journal of colloid and interface science*,*258*(1), 56-74.

Hill, R. J., Saville, D. A., & Russel, W. B. (2003). Polarizability and complex conductivity of dilute suspensions of spherical colloidal particles with charged (polyelectrolyte) coatings. *Journal of colloid and interface science*, *263*(2), 478-497.

Hobbie, E. K. (1998). Metastability and depletion-driven aggregation. *Physical review letters*, *81*, 3996-3999.

Hunter, R. J. (2001). *Foundations of Colloid Science*; Oxford University Press: New York, NY.

Hurd, A. J. (1985). The electrostatic interaction between interfacial colloidal particles. *Journal of Physics A: Mathematical and General*, *18*(16), L1055.

Hywel, M. & Green, N. (2003). *AC electrokinetics: colloids & nanoparticles*. No. 2. Research Studies Press.

Jackson, R. B., Jobbágy, E. G., Avissar, R., Roy, S. B., Barrett, D. J., Cook, C. W., ... & Murray, B. C. (2005). Trading water for carbon with biological carbon sequestration. *Science*, *310*(5756), 1944-1947.

Jiang P. & McFarl&, M. J., Wafer-scale periodic nanohole arrays templated from two-dimensional nonclose-packed colloidal crystals, *Journal of the American Chemical Society*, 2005, 127: 3710-3711.

Jiang, P., & McFarland, M. J. (2004). Large-scale fabrication of wafer-size colloidal crystals, macroporous polymers and nanocomposites by spin-coating.*Journal of the American Chemical Society*, *126*(42), 13778-13786.

Jiang, P., Bertone, J. F., Hwang, K. S., & Colvin, V. L. (1999). Single-crystal colloidal multilayers of controlled thickness. *Chemistry of Materials*, *11*(8), 2132-2140.

Jiang, X., Wang, B., Li, C. Y., & Zhao, B. (2009). Thermosensitive polymer brush-supported 4-N, N-dialkylaminopyridine on silica particles as catalyst for hydrolysis of an activated ester in aqueous buffers: Comparison of activity with linear polymer-supported version and effect of LCST transition. *Journal of Polymer Science Part A: Polymer Chemistry*, *47*(11), 2853-2870.

Johnston, D., & Wu, S. M. S. (1995). *Foundations of cellular neurophysiology*(pp. 392-395). Cambridge, MA: MIT press.

Jones, T. B. (2005). *Electromechanics of particles*. Cambridge University Press..

JunPark, B. (2010). Fluid-interface templating of two-dimensional colloidal crystals. *Soft Matter*, *6*(3), 485-488.

Kirby, B. (2010). *Micro-and nanoscale fluid mechanics: transport in microfluidic devices*. Cambridge University Press.

Kralchevsky, P. A., & Denkov, N. D. (2001). Capillary forces and structuring in layers of colloid particles. *Current Opinion in Colloid & Interface Science*, *6*(4), 383-401.

Krupke, R., Hennrich, F., Weber, H. B., Beckmann, D., Hampe, O., Malik, S., & Löhneysen, H. V. (2003). Contacting single bundles of carbon nanotubes with alternating electric fields. *Applied Physics A*, *76*(3), 397-400.

Lac, E., & Sherwood, J. D. (2009). Streaming potential generated by a drop moving along the centreline of a capillary. *Journal of Fluid Mechanics*, *640*, 55-77.

Lauffer, M. A., & Gortner, R. A. (1939). Electrokinetics. XXI. Electrokinetic Theory. Streaming Potential and the Electroösmotic Counter Effect. *Journal of Physical Chemistry*, *43*(6), 721-732.

Law, A. D., Auriol, M., Smith, D., Horozov, T. S., & Buzza, D. M. A. (2013). Self-Assembly of Two-Dimensional Colloidal Clusters by Tuning the Hydrophobicity, Composition, and Packing Geometry. *Physical review letters*,*110*(13), 138301.

Law, A. D., Buzza, D. M. A., & Horozov, T. S. (2011). Two-dimensional colloidal alloys. *Physical review letters*, *106*(12), 128302.

Lei, U., & Lo, Y. J. (2011). Review of the theory of generalised dielectrophoresis. *IET nanobiotechnology*, *5*(3), 86-106.

Levine, S., Levine, M., Sharp, K. A., & Brooks, D. E. (1983). Theory of the e lectrokinetic behavior of human erythrocytes. *Biophysical journal*, *42*(2), 127-135.

Li, D. (2004). *Electrokinetics in microfluidics* (Vol. 2). Academic Press.

Li, J., Zhang, Q., Peng, N., & Zhu, Q. (2005). Manipulation of carbon nanotubes using AC dielectrophoresis. *Applied Physics Letters*, *86*(15), 153116.

López- García, J. J., Horno, J., González-Caballero, F., Grosse, C., & Delgado, A. V. (2000). Dynamics of the electric double layer: Analysis in the frequency and time domains. *Journal of colloid and interface science*, *228*(1), 95-104.

López-García, J. J., Grosse, C., & Horno, J. (2003). Numerical study of colloidal suspensions of soft spherical particles using the network method: 1. DC electrophoretic mobility. *Journal of colloid and interface science*, *265*(2), 327-340.

López-García, J. J., Grosse, C., & Horno, J. (2003). Numerical study of colloidal suspensions of soft spherical particles using the network method: 2. AC electrokinetic and dielectric properties. *Journal of colloid and interface science*,*265*(2), 341-350.

López-García, J. J., Horno, J., & Grosse, C. (2003). Suspended particles surrounded by an inhomogeneously charged permeable membrane. Solution of the Poisson–

Boltzmann equation by means of the network method. *Journal of colloid and interface science*, *268*(2), 371-379.

Lumsdon, S. O., Kaler, E. W., & Velev, O. D. (2004). Two-dimensional crystallization of microspheres by a coplanar AC electric field. *Langmuir*, *20*(6), 2108-2116.

Lyklema, J. (2005). *Fundamentals of interface and colloid science: soft colloids* (Vol. 5). Academic press.

Ma, F., Wang, S., Smith, L., & Wu, N. (2012). Two-Dimensional Assembly of Symmetric Colloidal Dimers under Electric Fields. *Advanced Functional Materials*, *22*(20), 4334-4343.

Ma, H., & Dai, L. L. (2009). Structure of Multi-Component Colloidal Lattices at Oil− Water Interfaces. *Langmuir*, *25*(19), 11210-11215.

Mangelsdorf, C., & White, L. (1997). Dielectric response of a dilute suspension of spherical colloidal particles to an oscillating electric field. *Journal of the Chemical Society, Faraday Transactions*, *93*(17), 3145-3154.

Mason, T. G., & Bibette, J. (1996). Emulsification in viscoelastic media.*Physical review letters*, *77*(16), 3481.

Masschaele, K., Park B.J., Furst E.M., Fransaer J., & Vermant, J. (2010). Finite ion-size effects dominate the interaction between charged colloidal particles at an decane-water interface. *Physical Review Letters 105.4*: 048303.

Mikhael, J., Roth, J., Helden, L., & Bechinger, C. (2008). Archimedean-like tiling on decagonal quasicrystalline surfaces. *Nature*, *454*(7203), 501-504.

Morgan, F. D., Williams, E. R., & Madden, T. R. (1989). Streaming potential properties of Westerly granite with applications. *Journal of Geophysical Research: Solid Earth (1978–2012)*, *94*(B9), 12449-12461.

Motornov, M., Sheparovych, R., Lupitskyy, R., MacWilliams, E., Hoy, O., Luzinov, I., & Minko, S. (2007). Stimuli-Responsive Colloidal Systems from Mixed Brush-Coated Nanoparticles. *Advanced Functional Materials*, *17*(14), 2307-2314.

Nguyen, N. T., & Wereley, S. T. (2002). *Fundamentals and applications of microfluidics*. Artech House.

O'Brien, R. W., & White, L. R. (1978). Electrophoretic mobility of a spherical colloidal particle. *Journal of the Chemical Society, Faraday Transactions 2: Molecular and Chemical Physics*, *74*, 1607-1626.

Oettel, M., & Dietrich, S. (2008). Colloidal interactions at fluid interfaces.*Langmuir*, *24*(4),1425-1441.

Ohshima, H. (1994). Electrophoretic mobility of soft particles. *Journal of colloid and interface science*, *163*(2), 474-483.

Ohshima, H. (1995). Electrophoresis of soft particles. *Advances in colloid and interface science*, *62*(2), 189-235.

Ohshima, H. (2000). On the general expression for the electrophoretic mobility of a soft particle. *Journal of colloid and interface science*, *228*(1), 190-193.

Ohshima, H. (2005). Approximate expression for the electrophoretic mobility of a spherical colloidal particle covered with an ion-penetrable uncharged polymer Layer. *Colloid and Polymer Science*, *283*(8), 819-825.

O'Konski, C. T. (1960). Electric properties of macromolecules. V. Theory of ionic polarization in polyelectrolytes. *The Journal of Physical Chemistry*, *64*(5), 605-619.

Olbricht, W. L. (1996). Pore-scale prototypes of multiphase flow in porous media. *Annual review of fluid mechanics*, *28*(1), 187-213.

Painter, O., Lee, R. K., Scherer, A., Yariv, A., O'brien, J. D., Dapkus, P. D., & Kim, I. (1999).Two-dimensional photonic band-gap defect mode laser. *Science*,*284*(5421), 1819-1821.

Park, S. H., Gates, B., & Xia, Y. (1999). A Three-Dimensional Photonic Crystal Operating in the Visible Region. *Advanced Materials*, *11*(6), 462-466.

Pethig, R. (2010). Review article—dielectrophoresis: status of the theory, technology, and applications. *Biomicrofluidics*, *4*(2), 022811.

Pieranski, P. (1980). Two-dimensional interfacial colloidal crystals. *Physical Review Letters*, *45*, 569-572.

Pohl, H. A. (1978). *Dielectrophoresis*; Cambridge University Press: New York, NY.

Popović, B.D. (1971). *Introductory engineering electromagnetics*. Addison-Wesley Longman, Incorporated.

Prevo, B. G., & Velev, O. D. (2004). Controlled, rapid deposition of structured coatings from micro-and nanoparticle suspensions. *Langmuir*, *20*(6), 2099-2107.

Pyun, J., & Matyjaszewski, K. (2001). Synthesis of nanocomposite organic/inorganic hybrid materials using controlled/"living" radical polymerization. *Chemistry of Materials*, *13*(10), 3436-3448.

Ristenpart, W. D., Aksay, I. A., & Saville, D. A. (2003). Electrically guided assembly of planar uperlattices in binary colloidal suspensions. *Physical review letters*, *90*(12), 128303.

Saville, D. A. (2000). Electrokinetic properties of fuzzy colloidal particles.*Journal of colloid and interface science*, *222*(1), 137-145.

Sharp, K. A. & Brooks, D. E. (1985). Calculation of the electrophoretic mobility of a particle bearing bound poly-electrolyte using the nonlinear Poisson-Boltzmann equation. *Biophys. J. 47*, 563-566.

Sherwood, J. D. (2007). Streaming potential generated by two-phase flow in a capillary. *Physics of Fluids (1994-present)*, *19*(5), 053101.

Sherwood, J. D. (2008). Streaming potential generated by a long viscous drop in a capillary. *Langmuir*, *24*(18), 10011-10018.

Shilov, V. N. & Dukhin, S. S. (1970). Theory of Polarization of the Diffuse Part of a thin Double Layer at a Spherical Particle in an Alternating Electric Field. *Colloidal J., USSR, 32*, 90-95.

Somasundaran, P. (Ed.). (2006). *Encyclopedia of surface and colloid science*(Vol. 1). CRC Press.

Starov, V. M., & Solomentsev, Y. E. (1993). Influence of gel layers on electrokinetic phenomena: 1. Streaming potential. *Journal of colloid and interface science*, *158*(1), 159-165.

Starov, V. M., & Solomentsev, Y. E. (1993). Influence of gel layers on electrokinetic phenomena: 2. Effect of ions interaction with the gel layer.*Journal of colloid and interface science*, *158*(1), 166-170.

Stratton, J. A. (2007). *Electromagnetic theory* (Vol. 33). John Wiley & Sons.

Terfort, A., Bowden, N., & Whitesides, G. M. (1997). Three-dimensional self-assembly of millimetre-scale components. *Nature*, *386*(6621), 162-164.

Van Blaaderen, A., Ruel, R., & Wiltzius, P. (1997). Template-directed colloidal crystallization. *Nature*, *385*(6614), 321-324.

Velev, O. D., & Kaler, E. W. (1999). In situ assembly of colloidal particles into miniaturized biosensors. *Langmuir*, *15*(11), 3693-3698.

Vlasov, Y. A., Bo, X. Z., Sturm, J. C., & Norris, D. J. (2001). On-chip natural assembly of silicon photonic bandgap crystals. *Nature*, *414*(6861), 289-293.

Wall, S. (2010). The history of electrokinetic phenomena. *Current Opinion in Colloid & Interface Science*, *15*(3), 119-124..

Whitesides, G. M. (2006). The origins and the future of microfluidics. *Nature*,*442*(7101), 368-373.

Wu, T., Zou, G., Hu, J., & Liu, S. (2009). Fabrication of photoswitchable and thermotunable multicolor fluorescent hybrid silica nanoparticles coated with dye-labeled poly (N-isopropylacrylamide) brushes. *Chemistry of Materials*,*21*(16), 3788-3798.

Wunderlich, R. W. (1982). The effects of surface structure on the electrophoretic mobilities of large particles. *Journal of Colloid and Interface Science*, *88*(2), 385-397.

Wurmstich, B., & Morgan, F. D. (1994). Modeling of streaming potential responses caused by oil well pumping. *Geophysics*, *59*(1), 46-56.

Yezek, L. P., Duval, J. F., & van Leeuwen, H. P. (2005). Electrokinetics of diffuse soft interfaces. III. Interpretation of data on the polyacrylamide/water interface. *Langmuir*, *21*(14), 6220-6227.

Yue, P., Zhou, C., Feng, J. J., Ollivier-Gooch, C. F., & Hu, H. H. (2006). Phase-field simulations of interfacial dynamics in viscoelastic fluids using finite elements with adaptive meshing. *Journal of Computational Physics*, *219*(1), 47-67.

Zhao, H. (2011). Double-layer polarization of a non-conducting particle in an alternating current field with applications to dielectrophoresis. *Electrophoresis*,*32*(17), 2232-2244.

Zhao, H., & Bau, H. H. (2009). The polarization of a nanoparticle surrounded by a thick electric double layer. *Journal of colloid and interface science, 333*(2), 663-671.

Zhou, C. (2008). Simulations of interfacial dynamics of complex fluids using diffuse interface method with adaptive meshing.

Zhou, H., Preston, M. A., Tilton, R. D., & White, L. R. (2005). Calculation of the electric polarizability of a charged spherical dielectric particle by the theory of colloidal electrokinetics. *Journal of colloid and interface science, 285*(2), 845-856.

VITA

Graduate College

University of Nevada, Las Vegas

Sebastian Uppapalli

Degrees:

Master of Science, 2003

University of Nevada, Reno

Publications:

Uppapalli, S. & Zhao, H. (2014). Characterization of Streaming Potential due to Droplet Deformation in a Two-Phase Flow using Phase-Field-Method. *Under Review*.

Uppapalli, S. & Zhao, H. (2014). The Influence of Residual Charges on Electrostatic Interactions between Charged Colloidal particles at an Oil-Water Interface. *Accepted*.

Uppapalli, S., & Zhao, H. (2012). Polarization of a diffuse soft particle subjected to an alternating current field. *Langmuir*, *28*(30), 11164-11172.

Zhu, D., Nussbaum, N. J., Kuhns, H. D., Chang, M. C. O., Sodeman, D., Uppapalli, S., ... & Watson, J. G. (2009). In-plume emission test stand 2: emission factors for 10-to 100-kW US military generators. *Journal of the Air & Waste Management Association*, *59*(12), 1446-1457.

Gillies, J. A., Etyemezian, V., Kuhns, H., McAlpine, J. D., King, J., Uppapalli, S., ... & Engelbrecht, J. (2010). Dust emissions created by low-level rotary-winged aircraft flight over desert surfaces. *Atmospheric Environment*, *44*(8), 1043-1053.

Kuhns, H., Gillies, J., Etyemezian, V., Nikolich, G., King, J., Zhu, D., ... & Kohl, S. (2010). Effect of soil type and momentum on unpaved road particulate matter emissions from wheeled and tracked vehicles. *Aerosol Science and Technology*, *44*(3), 187-196.

Gillies, J. A., Kuhns, H., Engelbrecht, J. P., Uppapalli, S., Etyemezian, V., & Nikolich, G. (2007). Particulate emissions from US Department of Defense

artillery backblast testing. *Journal of the Air & Waste Management Association*,*57*(5), 551-560.

Dissertation Title: Simulations of Interfacial Electrokinetics with Applications to Microfluidic Systems.

Dissertation Examination Committee:

Chairperson, Hui Zhao, Ph. D.

Committee Member, Yitung Chen, Ph. D.

Committee Member, Robert Boehm, Ph. D.

Committee Member, Yingtao Jiang, Ph. D.

Graduate Faculty Representative, Mei Yang, Ph. D.